GEOLOGICA CARPATHICA, 2025, 76, 1, 37–53 https://doi.org/10.31577/GeolCarp.2025.03

Studying the 'water' content of the Firiza calc-alkaline basalts: Inferences from the Carpathian–Pannonian Region

ÁKOS KŐVÁGÓ[1,2,3,4,✉], MARINEL KOVACS[5], SZILVESZTER GERGELY[6], CSABA SZABÓ[2,3] and ISTVÁN JÁNOS KOVÁCS[2]

[1]Doctoral School of Earth Sciences, Faculty of Science, Eötvös Loránd University, Budapest, Hungary
[2]HUN-REN Institute of Earth Physics and Space Science, Sopron, Hungary
[3]Lithosphere Fluid Research Lab (LRG), Institute of Geography and Earth Sciences, Eötvös Loránd University, Budapest, Hungary
[4]Department of Petrology and Geochemistry, Faculty of Science, Eötvös Loránd University, Budapest, Hungary
[5]Technical University of Cluj-Napoca, North University Centre of Baia Mare, Baia Mare, Romania
[6]Department of Applied Biotechnology and Food Science, Faculty of Chemical Technology and Biotechnology, Budapest University of Technology and Economics, Budapest, Hungary

(Manuscript received November 6, 2024; accepted in revised form May 3, 2025; Associate Editor: Igor Broska)

Abstract: Firiza basaltic complex (FBC) is the final volcanic phase (8.1–7.0 Ma) of the Gutâi Volcanic Zone (GVZ) from the Neogene–Quaternary volcanic chain of the Eastern Carpathians (Romania). Nine small intrusions of the FBC crosscut older volcanic products (11.3–9.0 Ma) and consist of microporphyritic–aphanitic basalts. The volcanic rocks from GVZ, and FBC show typical arc-related geochemical features (calc-alkaline). Based on the chemical composition of the studied clinopyroxenes, the cores of the clinopyroxene phenocrysts and glomerocrysts are the most primitive (Mg#: 79–91) and alongside the olivine were the first crystallized phases. A deep magma source (22–30 km depth) in the lower crust near the MOHO (33–35 km depth in GVZ) is indicated by the crystallization pressures (~5.5–8.5 kbar) of the clinopyroxene cores. By studying the clinopyroxene cores with Fourier Transform Infrared spectrometry information for their structural hydroxyl content, 'water' content of their parental melt, and 'water' content of the mantle source region can be obtained. The structural hydroxyl content of the clinopyroxenes is relatively high (105–515 wt. ppm). The corresponding equilibrium melt 'water' contents (1.85–3.91 wt.%) and upper mantle source 'water' contents (2200–5200 wt. ppm) overlap with values reported from island arc basalts (IAB) and are higher than those from the alkali basalts from the Bakony–Balaton Highland Volcanic Field (BBHVF) (1.2–2.1 wt.% and 400–520 wt. ppm). The reason behind this is the different geodynamic positions of the two areas, the GVZ is in the close vicinity of a recent subduction whereas the BBHVF is not. This is the first work dealing with the 'water' content of calc-alkaline melts from the region.

Keywords: calc-alkaline basalts, magmatic 'water', clinopyroxene phenocryst, subduction, Carpathian–Pannonian region, p–T conditions, FTIR

Introduction

The nature and the evolution of the magmatic processes at the different levels in the lithosphere can be inferred from the study of rock-forming minerals. Clinopyroxene is a common early crystallising mineral in mafic to intermediate magmas and crystallises across a wide range of physical and chemical conditions (Ubide et al. 2019). Clinopyroxene is a highly sensitive mineral to pressure, temperature, and 'water' (if not otherwise specified, the term 'water' refers to all hydrous species in rocks: H^+, OH^-, H_2O) content (e.g., Putirka 2008; Mollo et al. 2013; Ubide & Kamber 2018; Ulmer et al. 2018; Marxer et al. 2022). In recent studies, clinopyroxene phenocrysts in basalts are generally used to constrain the 'water' content of the mafic melts and their source region (Xia et al. 2013a; Kovács et al. 2020; Radu et al. 2023). There are a growing number of observations that the source region of basaltic rocks can be hydrated to a very different extent from island arc basalts (IAB) to mid-ocean ridge basalts (MORB), representing the wettest and driest conditions respectively (Asimow et al. 2004; Dixon et al. 2004; Kushiro 2007;Grove et al. 2012; Plank et al. 2013; Collins et al. 2020). Studying the 'water' content of different rock-forming minerals (e.g., clinopyroxene, plagioclase, olivine) is a highly useful and widely accepted tool to constrain the hydration state of the source region (e.g., Xia et al. 2013a, 2017).

The Carpathian-Pannonian region (CPR) is home to several well-known alkali basaltic provinces: the Styrian Basin Volcanic Field (SBVF), the Little Hungarian Plain Volcanic Field (LHPVF), the Bakony–Balaton Highland Volcanic Field (BBHVF), the Nógrád–Gömör Volcanic Field (NGVF) and the Perșani Mountains Volcanic Field (PMVF) with the prospect of mapping the hydration state of the upper mantle beneath the basin system (Kovács et al. 2016, 2020; Patkó et al. 2019, 2025; Liptai et al. 2021). To date, there are two studies that have addressed this approach from the CPR, the BBHVF and NGVF, which demonstrated that the astheno-

✉ corresponding author: Ákos Kővágó
kovago.akos@epss.hun-ren.hu

spheric source is relatively wet (Kovács et al. 2020; Patkó et al. 2025). However, data from other alkali basaltic provinces and calc-alkaline basalts from the CPR are currently unavailable. Firiza basaltic complex, as the entire post-collisional magmatism from the GVZ was presumably affected by subduction in the Eastern Carpathians (Kovacs et al. 2017).

The objective of this study is to explore and understand the magmatic 'water' content of the FBC and to provide a comprehensive petrographic and geochemical background for this. For this, the structural hydroxyl content in the core of clinopyroxene phenocrysts and glomerocrysts will be analysed. Furthermore, the 'water' content of the parental melt and the source region will be inferred based on experimentally determined partition coefficients. Finally, with the knowledge of the hydration state of the source region, the results can be interpreted in the regional and global geodynamic context, and possible explanations can be inferred. The FBC is an ideal occurrence because these calc-alkaline basalts form relatively small intrusions, which cooled relatively fast. This allows the early crystallized clinopyroxenes to maintain their original structural hydroxyl. New data from the FBC will enable us to highlight the possible effects of subduction and regional geodynamic differences.

Geological background

The Gutâi Volcanic Zone (GVZ) is situated within the Neogene–Quaternary volcanic chain of the Eastern Carpathians. As part of the main volcanic range of the Carpathians, the GVZ developed in a highly complex tectonic zone at the contact between the two plates/megaunits, ALCAPA (ALpine–CArpathian–PAnnonian) and Tisza–Dacia of the Carpathian–Pannonian region (Csontos et al. 1992). The E–W striking Bogdan–Dragoş–Vodă fault system (Săndulescu et al. 1993; Gröger et al. 2008) represents the prolongation of the Mid-Hungarian Fault Zone (Csontos & Nagymarosy 1998) and developed in the south of GVZ and has accommodated several stages of extension (18.5–16 Ma), transpression (16–12 Ma), and transtension (12–10 Ma) deformation (Tischler et al. 2007, 2008; Gröger et al. 2008).

The GVZ is a transitional zone to the Călimani–Gurghiu–Harghita Volcanic Zone of the East Carpathians whose volcanism was entirely of post-collisional type (Seghedi & Downes 2011; Seghedi et al. 2023). Considering that the collision between the European plate/East European platform and the ALCAPA/Tisza Dacia plates took place between 11–10 Ma (see also the paper Harangi et al. 2024) the main phase of the intermediate volcanism in GVZ (11–9 Ma) can be considered post-collisional. Subduction in the area took place between 17–14 Ma and ended with the aforementioned collision (Harangi et al. 2024).

The complex volcanic activity of the GVZ occurred between 15.4 and 7.0 Ma (Pécskay et al. 2006). Two types of post-collisional volcanism were distinguished in the GVZ: (1) felsic/rhyolitic volcanism (initiated at ca. 15.4 Ma, Fülöp 2002, 2003) consisting of caldera-related ignimbrites and ignimbrite-related resedimented volcaniclastics interlayered with sedimentary deposits, and (2) intermediate/andesitic volcanism. Multiphase volcanism (13.4–7.0 Ma, Kovacs & Fülöp 2003) comprises four stages (Kovacs et al. 2017). The first two main stages (13.4–9.0 Ma) developed throughout the entire area of GVZ, which resulted in the formation of numerous volcanic structures, including composite volcanoes, effusive cones, extrusive domes, and associated intrusions. During the paroxysmal activity of the second main stage (11.6–9.0 Ma), subalkaline, predominantly medium-K basaltic andesites, andesites, and dacites were emplaced. A small-scale magmatic complex emplaced at 8.5–8.0 Ma (Laleaua Albă complex, Kovacs 2002) in the central-southern part of the GVZ is attributed to the third volcanic stage. The fourth volcanic stage (8.1–7.0 Ma, Edelstein et al. 1993; Kovacs et al. 2013a) is characterised by the development of small intrusive calc-alkaline basalt bodies in the central part of the GVZ, which marks the cessation of volcanic activity. This final magmatic event is the subject of the current paper (Fig. 1). The magmatic source of the Firiza basalts was the main deep magma reservoir ahat acted as a 'MASH zone' at the crust-mantle boundary in the GVZ with the involvement of lithospheric mantle over the entire time-interval of the intermediate volcanism (Kovacs et al. 2021).

Sampling and analytical methods

The magmatic complex of the fourth volcanic stage, the FBC, comprises nine small basaltic intrusions (50 to 300 m length and 20 to 100 m width) that outcrop along a NE–SW oriented alignment. These intrusions cross-cut the volcanic country rocks showing different ages (10.8–9.0 Ma) from the second main stage of the intermediate volcanic activity (Fig. 1 and Supplement S1). Results of the analyses conducted on the five samples selected from the FBC are presented in Table 1.

Petrography

The petrographic observations were conducted using a Nikon Eclipse LV100 POL polarising microscope. For the microphotographs, the NIS elements software in the Lithosphere Fluid Research Laboratory (LRG) of the Eötvös Loránd University (Budapest) was employed. For the purposes of petrography, 100 µm thin sections were used.

SEM-EDS and EMPA

The major element compositions and textural observations of the studied rock-forming minerals were analysed using scanning electron microscopy with energy dispersive X-ray spectroscopy (SEM-EDS) and electron microprobe analysis (EMPA) on the 100 µm thin sections used for petrography. The former system is a Quantax75 EDS-SDD combined with a Hitachi TM4000Plus microscope operating at the Eötvös Loránd University Faculty of Science Research and Instrument

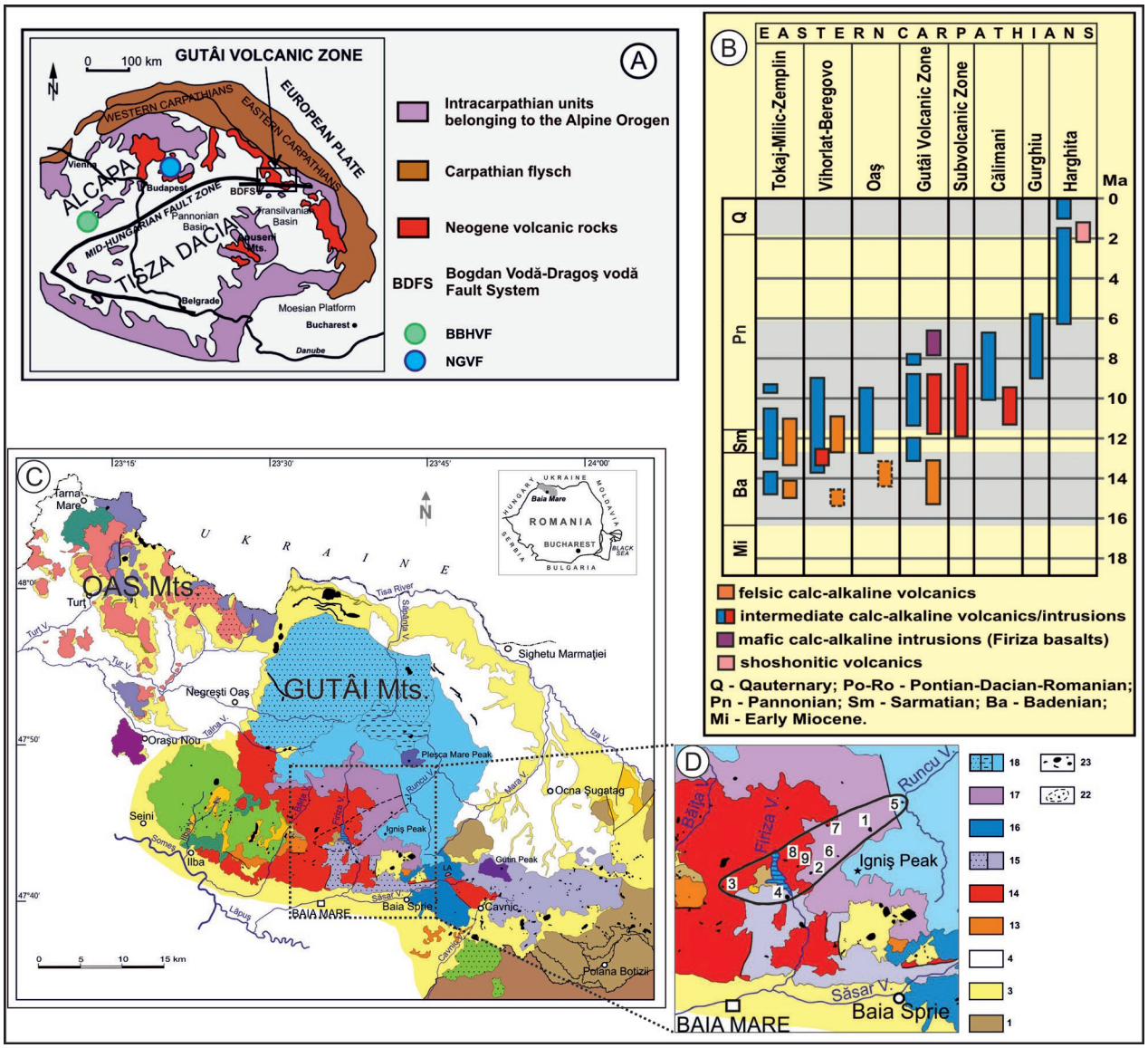

Fig. 1. Location, geology, and age distribution of the Gutai Volcanic Zone (GVZ) and Firiza Basaltic Complex (FBC). **A** — Location of the GVZ, BBHVF and NGVF in the Carpathian–Pannonian Region, on the eastern tip of the ALCAPA microplate close to the contact with the Tisza–Dacia microplates along the Bogdan–Dragoş–Vodă fault system (Săndulescu et al. 1993; Gröger et al. 2008); **B** — Age distribution of the volcanic products in the Eastern Segment of the Carpathian Volcanic belt with the Firiza calc-alkaline basalts highlighted with purple (after Edelstein et al. 1993; Kovacs et al. 2013a). **C** — Simplified geological map of the GVZ with the location of the FBC in the frame (shown in detail in D); **D** — Distribution of the calc-alkaline basalt intrusions of the FBC (for details see Supplement S1).

Core Facility (ELTE-FS-RICF). The settings were 15 kV accelerating voltage, 200 pA beam current, and 30 s counting times. The EMPA employed a JEOL JXA-8100 electron microprobe, equipped with five wavelength dispersive spectrometers (WDX), at the Institute of Mineralogy and Petrography from the University of Innsbruck (Austria), with the following settings: 5 kV acceleration voltage, 10 nA beam current and 20 s peak and 10 s background counting time. The following standards were employed: jadeite for Na, orthoclase for Mg, MgO for K, diopside for Ca, rhodonite for Mn, orthoclase for Si, corundum for Al, chromite for Cr, rutile for Ti, and almandine for Fe. For further details on the analytical methodology employed in the mineral chemistry data of Fir4b, please refer to Kovacs et al. (2021).

The reliability of the SEM-EDS measurements was tested by re-measuring with SEM-EDS in the same spots as with the EMPA and then comparing the results. In order to obtain more comprehensive data, different minerals (pyroxene, olivine, plagioclase, and oxides) and different thin sections were measured. The evaluation of the data indicates that the SEM-EDS mineral chemistry data are satisfactory for petrogenetic purposes (see Supplement S2). The SEM-EDS and EMPA measurements were conducted on the same thin sections as the petrographic studies.

Bulk rock chemistry

The bulk rock chemical analysis for the sample Fir4a was conducted in the laboratory of the Mining and Geological Survey of Hungary. The calculation of the loss on ignition (LOI) was performed after heating the sample at 1050 °C and then calculated based on weight difference. The sample was pulverised below 63 microns and then prepared with lithium borate fusion for chemical analysis. The pulverised, homogeneous sample was weighed into a platinum crucible, with 0.5 g of the sample being placed therein. Subsequently, 1.16 g of $LiBO_2$ was added to the crucible, which was then covered with a platinum lid and gradually heated in a furnace up to 1060 °C. This process of heating and fusing the contents of the crucible was carried out for 30 minutes. Once the crucible had cooled, it was placed in a 100 ml glass beaker, covered with a sufficient amount of deionised water (approximately 50 ml) and 10 ml of 1:1 HCl. The fusion melt was dissolved using a magnetic stirrer plate. The solution was transferred into a volumetric flask and filled up to 250 ml. This diluted sample was then analysed. For the main elements, a Jobin Yvon Ultima 2C ICP-OES was employed, while for the trace elements, a Perkin–Elmer SCIEX ELAN DRC II ICP-MS was utilised. The accuracy of the ICP-OES was ±2 % for Si, Al, Fe, Ca, Sr and ±5 % for Ti, Mn, Mg, Na, and K. In the case of the ICP-MS, the accuracy was ±2 % for Rb, Y, Zr, La, Ce, Pr, Nd, Pb, and ±5 % for Nb, Cs, Sm, Gd, Dy, Er, Yb, Th.

For samples Fir1, 2, 3a, and 6, please refer to the analytical details presented in Kovacs et al. (2017) as Fir2, 3a and 5 are published from Kovacs et al. (2017) and Fir1 is unpublished data measured in the same laboratory.

Table 1: The analyses performed on the samples from the FBC. Data from literature: *Kovacs et al. (2017); **Kovacs et al. (2021).

Intrusions	Location	Sample	Petrography	Bulk rock chemistry	Mineral chemistry	FTIR
1	Pestilor Valley	Fir1	X	X	X	X
2	Berdu Ridge	Fir2	X	X*	X	X
3	Tocastru zone	Fir3a, Fir3b	X X	X*	X X	X X
4	Firiza lake	Fir4a, Fir4b	X X	X	X X**	X
5	Runcului Valley	Fir5	X			
6	Vidra Valley	Fir6	X	X*		
7	Băii Valley	Fir7	X			
8	Corneşiţa Valley	Fir8	X			
9	NW of the Corneşiţa Valley	Fir9	X			

FTIR measurements

The structural hydroxyl content of the nominally anhydrous minerals (NAMs) was determined using micro-Fourier Transform Infrared Spectrometry (micro-FTIR). The measurements were conducted on a Bruker Vertex 70 spectrometer coupled with a Bruker Hyperion 1000 infrared microscope at the Institute for Geological and Geochemical Research, Research Center for Astronomy and Earth Sciences (Budapest) for the sample Fir4a. For the remaining samples, the measurements were conducted at the Budapest University of Technology and Economics using a Spotlight400 microscope connected to a Spectrum400 spectrometer. Additionally, control measurements were performed on the Fir4a sample to monitor potential interlaboratory differences, which were not observed.

Double-polished sections with a thickness of 200–300 µm were prepared for the micro-FTIR analyses. The double-polished slabs were removed from the glass using acetone. To eliminate surface adsorbed water on the samples, the samples were heated at 90 °C for one hour in the presence of silica gel. During the measurement, the laboratory was air-conditioned to maintain a stable temperature throughout the measurements. For filtering out atmospheric interference, atmospheric correction and frequent background measurements were made. The settings of the measurements were as follows: an aperture of 50×50 µm, a spectral resolution of 4 cm^{-1}, 128 scans, and a spectral range of 400–4000 cm^{-1}.

The recorded spectra were processed using OPUS 7.2 software. For the baseline correction the concave rubber band method was used with 1 iterations and 64 baseline points. The selected spectra were averaged first in each grain and then from the grains these averaged for the whole sample. The integration for the structural hydroxyl region was made between 3700–3100 cm^{-1} with B type integration for all samples. This B-type integration method considers the area between the line connecting the intersections of the integration limits with the spectrum itself.

To estimate the structural hydroxyl content of the clinopyroxene phenocrysts, the following equation (1) was applied, where the concentration of the absorbing molecule is proportional to the integrated molar absorbance according to the Beer–Lambert law. In Equation (1), c is the concentration of the absorbing molecule (in wt.%), t is the thickness (in cm) where the uncertainty is ±1 µm for the analysed thickness range, and ε is the integrated molar absorption coefficient for augite. The molar absorption coefficient for augite is 38,300 ±1700 L/(mol $H_2O \cdot cm^2$) (Bell et al. 1995). The molar weight of the molecular 'water' is 18.02 g/mol, and the density of the clinopyroxene is 3256 (g/L) (Bell et al. 1995).

$$c_{H_2O} = \frac{A^{tot} \cdot M_A}{\varepsilon \cdot t \cdot \rho} \cdot 100 \quad (1)$$

The structural hydroxyl content is expressed in H_2O equivalent in wt. ppm. The total polarized absorbance is estimated using the method of Kovács et al. (2008) and Sambridge et al. (2008), whereby the total polarized absorbance is three times the average integrated unpolarized absorbance when the maximum linear unpolarized absorbance is less than 0.15

absorbance unit. In order to calculate the average absorbance spectra, a minimum a few, and optimally more than ten unoriented grains are required, with different crystallographic orientations with respect to the direction of the incoming light. The number of the considered unoriented sections varies with the extent of anisotropy.

A minimum of four unpolarized measurements were taken from each analysed sample. Xia et al. (2013b) demonstrated that the uncertainty in the structural hydroxyl content is below 10 % and less than 30 % even if only one crystallographic orientation is available for pyroxenes. Patkó et al. (2019) pointed on that if five unoriented crystals are available, the cumulative uncertainty can be reduced to below 10 %. The error propagation method described in Patkó et al. (2019) Supplementary Table 1 (based on Liu et al 2006) was performed for our samples as well. In the mentioned method the resulting error contains the uncertainties in the integral molar extinction coefficient (ε), density (ρ), sample thickness (t) and total polarized absorbance (A_{tot}) – assumed to be estimated based on n random measurements on unoriented grains with unpolarized radiation (n=the number of analysed grains for each sample). The resulting error for the lowest number of 4 grains is 7 %, but to give a more conservative estimate we used 10 % error uniformly in our work. For the calculation details see Supplement S12. To assess the homogeneity of the structural hydroxyl content, transect measurements were conducted on the clinopyroxenes studied in this paper.

Selection criteria of clinopyroxene for FTIR

In order to accurately determine the water content of the most primitive parental melt, certain criteria must be imposed on the clinopyroxene crystals. The clinopyroxene crystals must represent the earliest stage of crystallisation in equilibrium with a parental melt, therefore the most suitable parts of early clinopyroxene phenocrysts or glomerocrysts are the cores. If these clinopyroxenes are zoned, cores are preferred for FTIR, as they are assumed to better preserve the original hydroxyl content. Furthermore, from a geochemical perspective, the Mg# of clinopyroxenes should be higher than 75, with a preference for values above 80, as previously demonstrated in studies by Liu et al. (2016) and Xia et al. (2013b). It is essential that the clinopyroxene grains are free of any inclusions, alterations and exsolution lamellae.

Results

Petrography

The selected FBC rocks are composed of clinopyroxene, plagioclase, rare olivine, and very rare amphibole phenocrysts in descending order. The same mineral assemblage occurs in the groundmass, with some orthopyroxenes and oxide minerals. A distinctive feature of the studied basalts is the presence of numerous clusters comprising exclusively clinopyroxenes or clinopyroxenes with olivine or clinopyroxenes with plagioclases. The FBC basalts exhibit a transition from fine aphanitic to porphyritic texture, with fluidal character, particularly in the groundmass. They can also contain brownish glass (Fig. 2 and Supplement S3).

The clinopyroxene phenocrysts are subhedral–euhedral, measuring between 350 and 770 μm in size, whereas the glomerocrysts are euhedral–subhedral, measuring between 410 and 480 μm in size. Both the phenocrysts and the glomerocrysts are unaltered and contain silicate melt inclusions (SMI) and oxide minerals. Many of the clinopyroxenes show distinct zoning textures. The groundmass clinopyroxene crystals are subhedral euhedral (20–60 μm in size) and all are fresh.

Plagioclase is the second most common phenocryst. They are euhedral-subhedral tabular (600–1150 μm in size) with complex zoning, simple twinning and sometimes sieve-textured cores without resorption rims (see Supplement S3). Sometimes plagioclases are present in the clusters with clinopyroxenes, with individual plagioclase glomerocrysts ranging from 400 to 800 μm in size. In the groundmass, plagioclase usually occurs as euhedral subhedral crystals (10–100 μm in size).

Olivine phenocrysts (mostly euhedral forms of 400–1100 μm in size) are usually partially or completely altered to iddingsite. The fresh olivine shows no zoning but contains a few SMIs and oxide minerals as inclusions (Fig. 2 and Supplement S3). The same features can be observed for the glomerocrystic olivine. The groundmass olivine crystals are mostly anhedral (10–40 μm in size) and fresh.

Orthopyroxene is found in the groundmass, sometimes as corona around the groundmass olivine crystals.

The scarce amphibole appears as large subhedral slightly resorbed phenocrysts containing clinopyroxene inclusions (Kovacs et al. 2021).

The oxide minerals are euhedral to anhedral crystals in the groundmass, usually associated with the clinopyroxenes, especially in the intergranular textures.

Xenocrystic quartz crystals are found in some samples, often resorbed, fractured and surrounded by clinopyroxene corona. In numerous instances within the boundary zone between quartz crystals and clinopyroxenes, brownish glass is observed (see Supplement S3).

Whole rock geochemistry

The geochemical characterisation of the studied FBC samples was performed on the basis of five bulk rock analyses representing samples from five different basaltic intrusions (Fig. 1, Supplement S4). The alkali basalts from the BBHVF and NGVF were used as comparison from the region as they are well studied petrologically and their water content was determined with the same methodology (Kovács et al. 2020; Patkó et al. 2025).

Rocks from the FBC lie within the basalt field in the total alkali-silica (TAS) diagram (except for sample Fir4a that contains frequent quartz xenocrysts, which lies in the basaltic

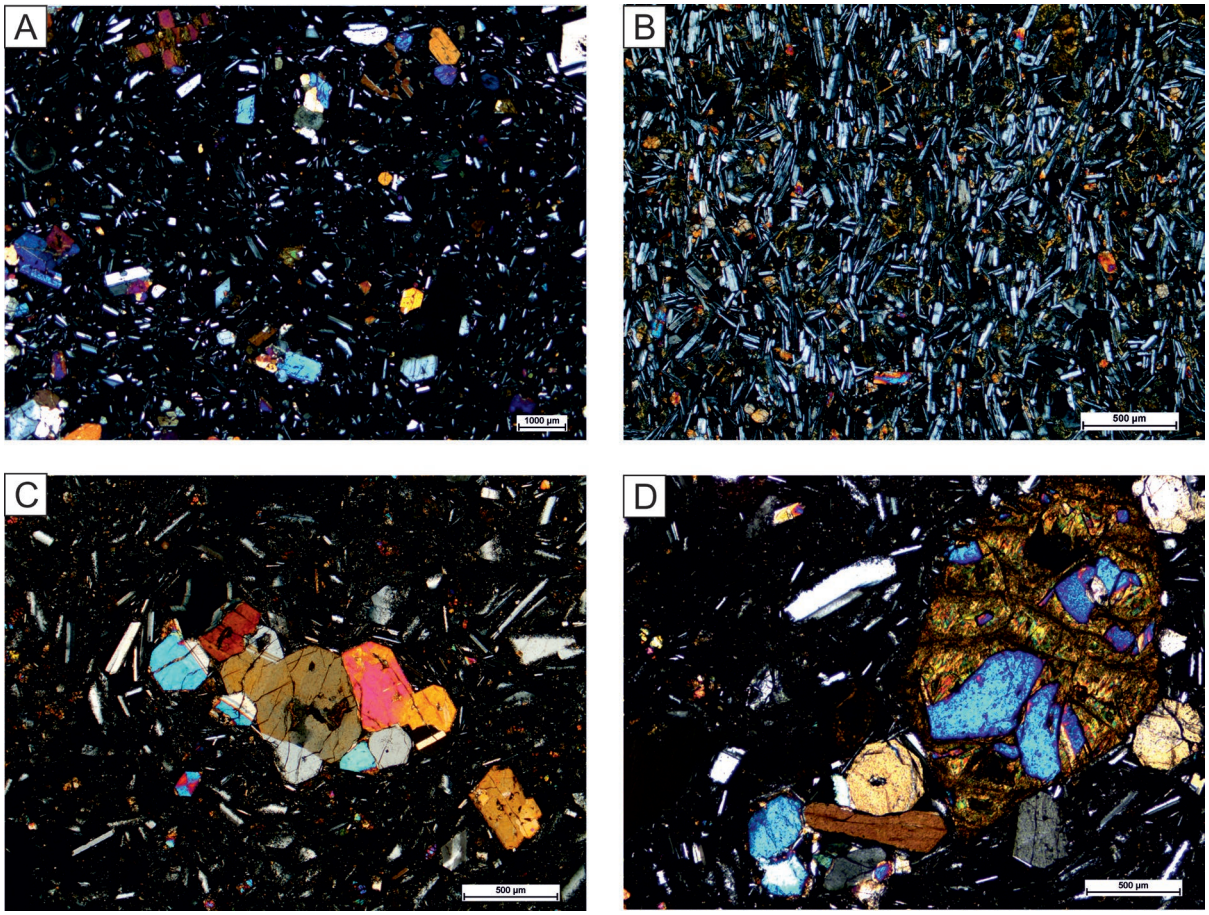

Fig. 2. Photomicrographs of the Firiza basalts. **A** — General view of a microporphyritic basalt (7134K); **B** — Fluidal texture in an aphanitic basalt (1491-VO); **C** — Cluster of exclusive clinopyroxenes (glomerocrysts) (7134K); **D** — Cluster of clinopyroxenes and olivine (partly altered) (7134K).

andesite field, Fig. 3A) and are classified as medium to high-K rocks according to the Peccerillo–Taylor diagram (Fig. 3B). In comparison, data from the alkali-basalts from the CPR (Embey-Isztin et al. 1993; Dobosi & Jenner 1999; Harangi et al. 2015) fall into the trachybasalt, tephrite-basanite and foidite fields in the TAS diagram and into the shoshonitic basalt field in the Peccerillo–Taylor diagram. The FBC basalts also fit the description of high-alumina basalts (Kuno 1960).

The major and trace elements show negative correlations with silica content only for some elements (MgO, CaO, Sc) and positive correlations for alkalis (Na+K) and Rb due to the small range of variation of Si.

The chondrite-normalised REE diagram shows small LREE enrichments, small negative Eu anomalies and flat HREE pattern (Fig. 3C), compared to those of the CPR alkaline basalts, which show greater enrichment in LREE and no negative Eu anomaly. The studied rocks of the FBC show enrichment in large ion lithophile elements (LILE), depletion in Nb, positive Pb and small negative P, Ti and Zr anomalies (Fig. 3D), which are not characteristic of the CPR alkaline basalts (Fig. 3D).

The characteristics of the studied FBC rocks outlined in the two figures are typical of subduction zone-related volcanism and are similar to all lithologies from the GVZ reported by Kovacs et al. (2017).

Clinopyroxene chemistry

The studied clinopyroxenes (phenocrysts and glomerocrysts; Table 2) are represented by diopside and augite, according to the IMA classification (Morimoto et al. 1988; Fig. 4) Furthermore, in case of the clinopyroxenes, only those with Mg# higher than 75 are focused on furthermore (Supplement S5), according to the selection criteria used for the FTIR analysis (Liu et al. 2016; Xia et al. 2013b). Both textural types of clinopyroxenes have similar narrow compositional ranges: $Wo_{40–50}$ $En_{40–48}Fs_{5–14}$ for glomerocrysts and $Wo_{41–49}En_{39–50}Fs_{4–14}$ for phenocrysts.

The SiO_2 content ranges between 47–54 wt.% with the majority (1st quartile–3rd quartile) is in the range of 49.7–51.4 wt.%. Al_2O_3 values range from 1.05–7.96 wt.% with most analyses ranging between 3.52–5.04 wt.%. Mg# values are in the range of 75–90, but typically between 80 and 85 (Fig. 5). The FeO and MgO shows strong negative correlation, with lower FeO for the cores compared with the rims

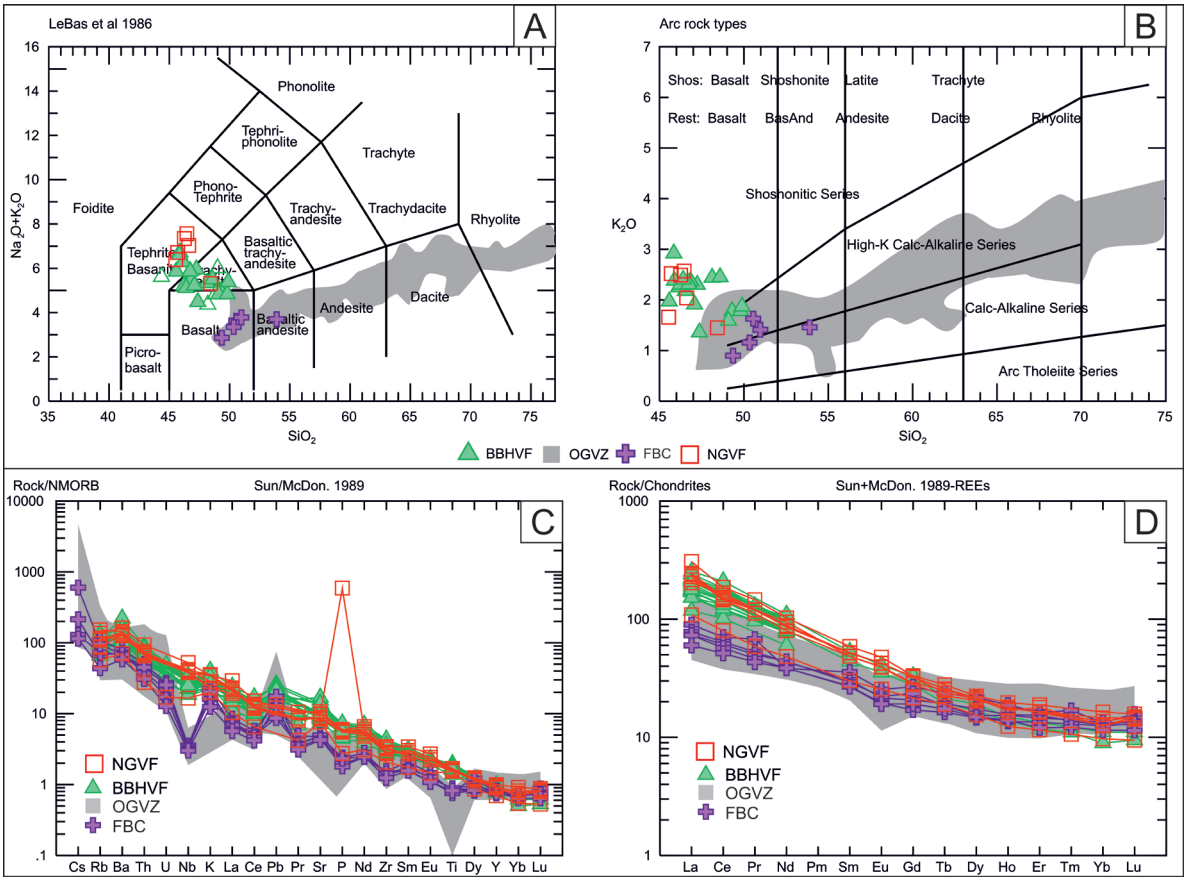

Fig. 3. Distribution of the Firiza Basaltic Complex rocks (purple crosses) in TAS (Le Bas et al. 1986; **A**), (Peccerillo & Taylor 1976; **B**), N-MORB normalized trace elements spider diagram **(C)**, and Chondrite-normalized rare earth elements diagram **(D)** compared to the Guta Volcanic Zone rocks and the alkali basalts from the; BBHVF: Bakony–Balaton Highland Volcanic Field; NGVF: Nógrád–Gömör Volcanic Field, Banat.

Table 2: Chemical composition of representative clinopyroxene phenocrysts and glomerocrysts.

Sample	Textural type	SiO_2	TiO_2	Al_2O_3	Cr_2O_3	FeO total	MnO	MgO	CaO	Na_2O	K_2O	Mg#
Fir1	G	50.4	0.68	4.55	0.22	6.63	0.09	15.1	21.9	0.31	0.07	87
Fir1	P	51.2	0.50	3.59	0.12	6.94	0.14	15.9	21.3	0.31	0.11	87
Fir2	G	50.8	0.70	3.89	0.15	8.09	0.25	15.0	21.0	0.30	0.07	81
Fir2	P	51.4	0.65	4.38	0.17	6.00	0.20	15.8	21.2	0.20	0.02	83
Fir3a	G	51.2	0.70	4.91	0.14	6.23	0.08	15.4	21.0	0.31	0.08	82
Fir3a	P	48.4	1.10	5.68	0.12	9.37	0.12	13.8	21.1	0.22	0.15	81
Fir3b	G	51.9	0.56	3.30	0.14	5.41	0.09	16.0	22.4	0.14	0.00	86
Fir3b	P	52.0	0.54	2.95	0.14	5.88	0.12	15.7	22.4	0.32	0.14	87
Fir4a	G	51.1	0.59	3.84	0.69	6.14	0.10	15.4	22.0	0.20	0.00	84
Fir4a	P	51.0	0.63	3.80	0.36	7.24	0.15	15.2	21.4	0.21	0.00	82
Fir4b	G	52.2	0.46	3.29	0.13	5.68	0.13	16.1	21.5	0.18	0.00	84
Fir4b	P	52.2	0.48	3.32	0.13	5.46	0.11	16.1	21.7	0.18	0.00	84

(Fig. 5A, B). In contrast, CaO presents strong positive correlation with Mg#, with higher values in the clinopyroxene cores (Fig. 5C, D). Negative correlation between TiO_2 and Mg# is observed, especially in the clinopyroxene cores (Fig. 5E, F). Cr_2O_3 and Mg# show only weak positive correlation for the highest Mg# corresponding to the cores of the two clinopyroxene textures.

The chemical data, shown in the diagrams in Fig. 5, prove that the cores of the clinopyroxene phenocrysts and glomerocrysts are the most primitive types, with the highest Mg#, CaO and Cr_2O_3, and the lowest FeO and TiO_2 contents.

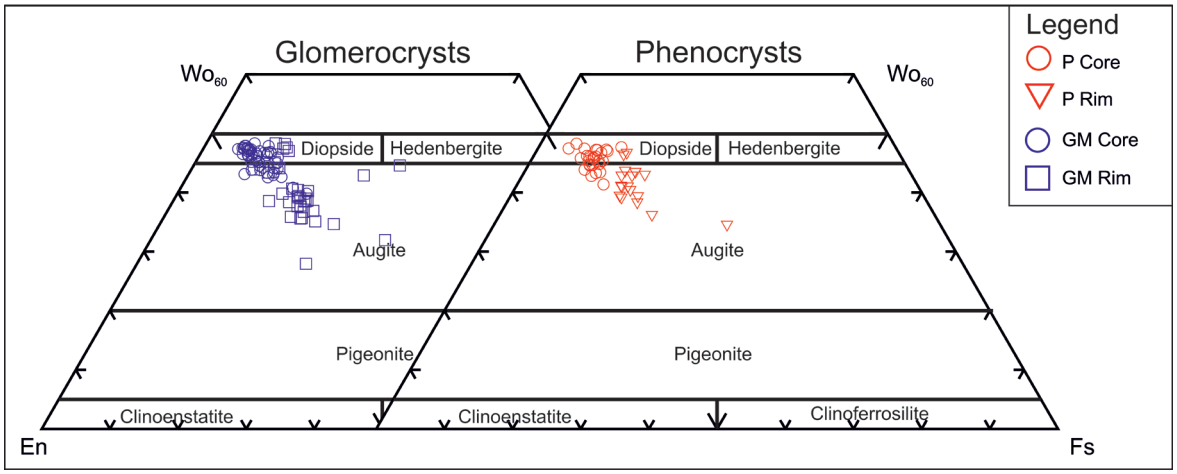

Fig. 4. Distribution of the clinopyroxenes from FBC in the quadrilateral classification diagrams (Morimoto et al. 1988).

Clinopyroxene geothermobarometry

The thermometer and barometer of Putirka (2008) were used to calculate the pressure and temperature of clinopyroxene crystallisation. For testing the equilibrium between clinopyroxene and the selected liquid, the recommendations of Putirka (2008) and Neave & Putirka (2017) were followed: the values of the Fe–Mg equilibrium test (Eq. 35: $KD_{cpx-liq}$ should be 0.27±0.03) for the clinopyroxene-liquid pairs considered to be within 10 % and the diopside–hedenbergite (DiHd) component equilibrium test (the predicted and observed values of the clinopyroxene DiHd component) to be within 20 %. In our calculation, the clinopyroxene-liquid pairs are selected within 10 % of the DiHd component equilibrium values using a one-to-one line diagram (Supplement S7) and matching with 0.27±0.03 $KD_{cpx-liq}$ values (Eq. 35). The pressures are calculated using Eq. 31 (standard error of estimate (SEE)=±2.9 kbar) and the temperatures using Eq. 33 (SEE=±45 °C) of the Putirka (2008) models (see Supplement S6).

The pressure values range between 4.3–9.3 kbar and the temperature values between 1063–1177 °C, the main majority pressure and temperature values between 5.5–8.5 kbar and 1100–1170 °C respectively, these values represent minimum estimates. The pressure vs. temperature plot shows a general positive correlation for the textural mineral types considered (phenocrysts and glomerocrysts, Fig. 6A). The analysed clinopyroxene crystals (phenocrysts and glomerocrysts) have pressure and temperature values that vary over a wide range. The pressure and temperature used are the weighted averages calculated for each textural mineral type from all six basalt samples examined (Table 3, Fig. 6). Considering the pressure values of each analysed textural mineral type, the ranges are quite similar (P=5.9–7.4 kbar; G=6.6–6.9 kbar) and as a whole in the SEE of the Putirka (2008) geobarometer (±2.9 kbar). The temperature values range between 1112–1151 °C, which are also in good agreement with the SEE of the Putirka (2008) geothermometer (±45 °C). The temperature values of the glomerocrystic clinopyroxenes are slightly higher than those of the phenocrysts, suggesting that these textural types crystallised at slightly higher temperatures (the first crystallised clinopyroxene crystals, see Fig. 6A and Table 3).

Overall, a range of 3 kbar of crystallisation pressure (5.5–8.5 kbar) can be assumed for the clinopyroxenes of the Firiza basalts, corresponding to a magma storage depth of 20–30 km, taking into account the average crustal density of 2700 kg/m^3 in the Gutâi volcanic zone according to Kovacs et al. (2021). The pressure–temperature data obtained for the clinopyroxenes in this study are consistent with those previously published by Kovacs et al. (2021).

'Water' content of the basalt and the mantle source

FTIR measurements of clinopyroxenes

Clinopyroxenes in all five of the studied samples (Table 1) were measured, and representative unpolarized average infrared spectra normalized to 1 cm are illustrated in Fig. 7.

Three major absorption bands were observed in the structural hydroxyl region, these are the bands around 3630, 3520 and 3470 cm^{-1}. The intensity of the absorption varies between the samples. The highest absorption can be observed in the Fir3a sample, where the 3630 cm^{-1} band shows the strongest absorbance. The second highest is the 3470 cm^{-1} band, and the third is the 3520 cm^{-1} band. However, in this sample, there is a notable contribution of molecular water, which manifests as a bulge visible between 3200 and 3300 cm^{-1}. With regard to the samples Fir4a and Fir3b, the relative intensity of the absorption bands demonstrates continuous decrease from the higher wavenumbers towards the lower ones. These samples can be categorised as so-called type 1 clinopyroxenes described by Patkó et al. (2019) as spectra characterized by decreasing intensities of peaks from higher towards lower wavenumbers. In the Fir2 basalt, the 3520 and 3470 cm^{-1} bands exhibit high degree of similarity in their respective

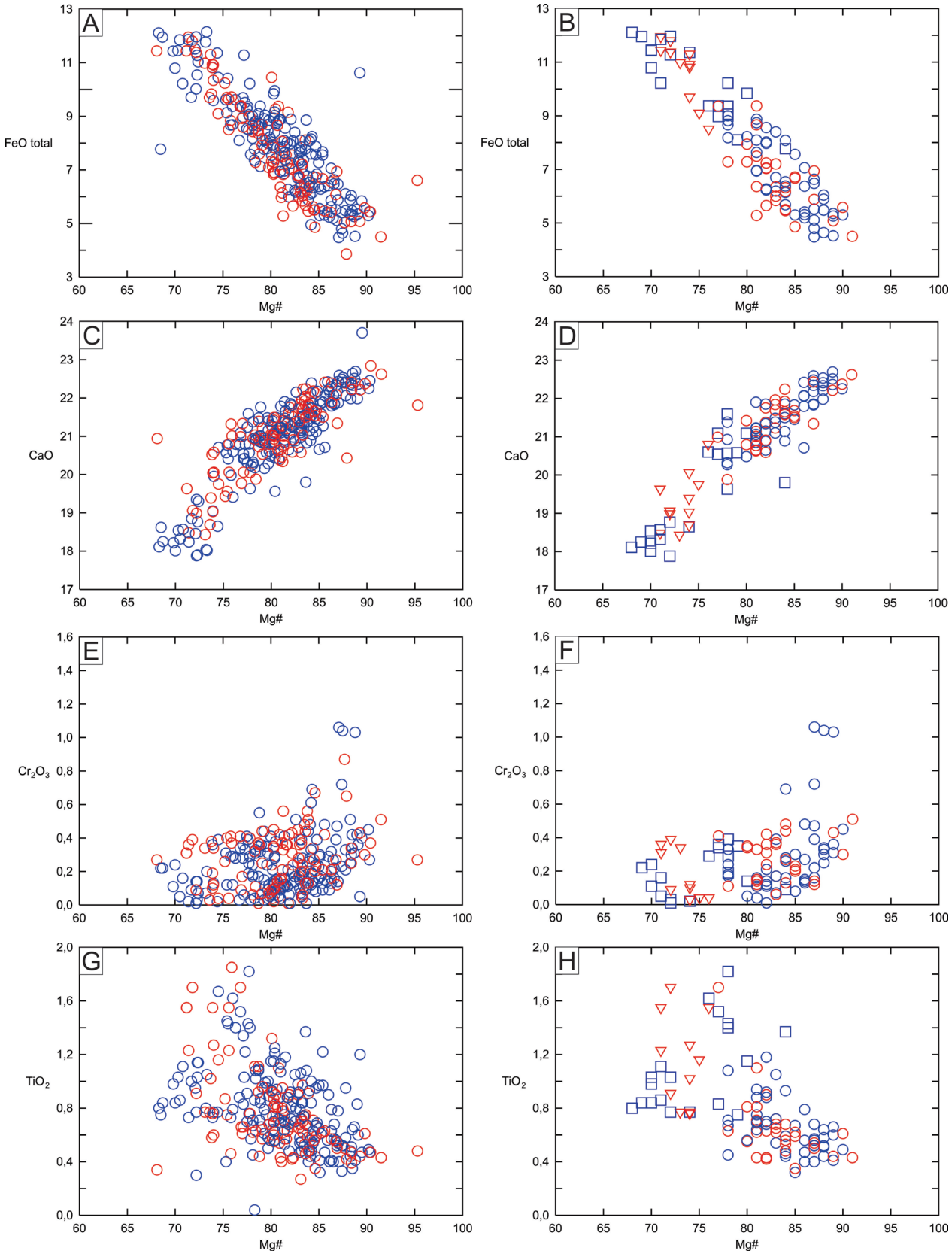

Fig. 5. Major elements vs. Mg# values in the clinopyroxene phenocrysts (red symbols) and glomerocrysts (blue symbols). On the diagrams from the right side, only the values of the cores (circle symbols) and rims (triangle and square symbols) are plotted. The transition zone values in between the cores and rims typically assigned to lower Mg# cores.

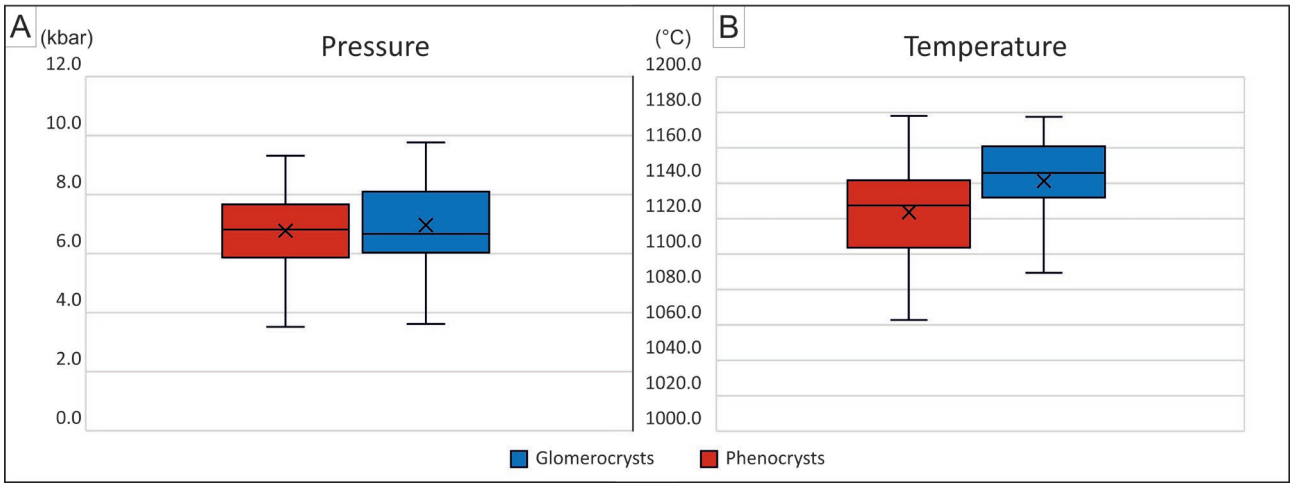

Fig. 6. Pressure (**A**) and Temperature (**B**) variations of the studied glomerocrysts and phenocrysts from the FBC displayed on a box and whiskers plot. The glomerocrysts display higher temperatures and slightly higher pressures compared to the phenocrysts.

Table 3: Calculated pressures and temperatures (as weighted averages) for the analysed textural mineral types from the FBC (P – phenocryst; G – glomerocryst).

Sample	Textural mineral-type	Number of analyses	Pressure (kbar)	Tempearature (°C)
Fir1	P	30	7,3	1127
	G	28	6,9	1133
Fir2	P	13	7,4	1128
	G	21	6,9	1151
Fir3a	P	17	6,8	1114
Fir3b	P	12	6,1	1112
	G	8	6,8	1129
Fir4a	P	20	5,9	1119
	G	8	6,6	1142
Fir4b	P	32	6,5	1126

intensities, with the 3630 cm^{-1} band exhibiting slight decrease in intensity. In the Fir1 basalt sample, relatively low absorption can be observed, which is close to the detection limit.

The calculated structural hydroxyl contents of the clinopyroxenes averaged by basalt samples are as follows: Fir3a: 1153±115.3 wt. ppm, Fir4a: 515±51.5 wt. ppm, Fir3b: 340 ±34 wt. ppm, Fir2: 284±28.4 wt. ppm, Fir1: 105±10.5 wt. ppm (Supplement S8). The measurement spots in the studied grains are located in the cores and transition zones of the crystals, the rims are typically represented by a thin zone on the edge of the clinopyroxenes. Furthermore, transect measurements were conducted with the objective of identifying diffusion profiles within the crystals. However, these measurements did not detect signs of diffusion for the core and transition zone regions, which were used for the calculations.

For the sample Fir3a we can see a broad, significant elevation of the baseline attributed to the high contribution of molecular 'water' (Biró et al. 2016) and in the case of sample Fir1 we can see a very prominent noise on the spectra and also a very low structural hydroxyl content, therefore from the calculations of melt and source region 'water' contents we excluded these two samples.

'Water' content of the basaltic melt

To calculate the 'water' content of the melt in equilibrium with the studied clinopyroxenes, the composition dependent partition coefficient of O'Leary et al. (2010) were used. The partition coefficient can be calculated by the equation (10) from O'Leary et al. (2010), using the cation fractions of the clinopyroxenes:

$$lnD_{H_2O}^{cpx-melt} = -4.2 + 6.5 \cdot X_{Al^{IV}}^{cpx} - 1 \cdot X_{Ca}^{cpx} \quad (2)$$

Al (^{IV}) is calculated the following way:

$$^{IV}Al^{3+} = \frac{1}{2}\left(\Sigma Al^{3+} - Na^{+}\right) \quad (3)$$

$$c_{melt}^{H_2O} = \left(\frac{c_{cpx}^{OH}}{D_{H_2O}^{cpx-melt}}\right)/10000 \quad (4)$$

The effects of pressure and temperature on the partition coefficient are negligible (Kovács et al. 2020) and were not considered. As the 'water' content in equilibrium with the studied clinopyroxenes can be increased by fractionation and lead to an overestimation of the 'water' content in the parental, it should be taken into account (Kovács et al. 2020).

As the exact values for the fractionation of the melts are not known, the equilibrium 'water' content was corrected during the calculation with various degrees of fractionation, namely 0, 5, 10, 15, 20 and 25 %.The resulting water contents, with error margin of 10 %, and considering a 20 % fractionation, were between 1.85 and 3.91 wt.% H_2O (Fig. 8A) for the selected samples (Fir2, 3b, 4a). These values are thought to be more conservative and were therefore used for further calculations.

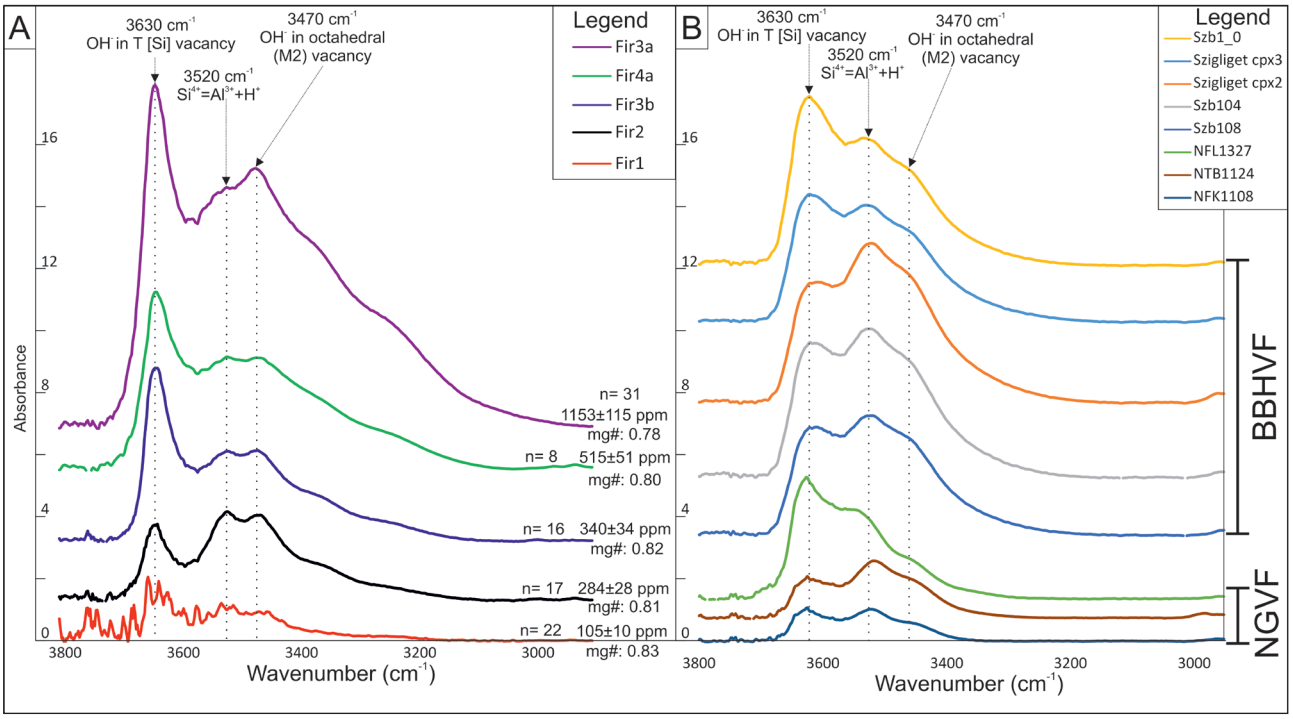

Fig. 7. The FTIR spectra recorded in this study (**A**) and from Kovács et al. (2016) and Patkó et al. (2019) (**B**) normalized to 1 cm. The important absorption bands are marked on both sets of spectra, and on the FBC are also marked the number of measurements (n), mg#, and OH-content (±values representing the 10 % uncertainty).

'Water' content in the mantle source

The objective of these calculations is to determine the 'water' content of the mantle source of the FBC basalts, given the geodynamic situation and previous works which indicate that the primitive melts originate from a mantle source (Kovacs et al. 2017) and the high Mg content of the clinopyroxene cores (79–91), which also supports this hypothesis.

The 'water' content of the mantle source was determined using the following equations (where Eq. 5 is for modal batch and Eq. 6 is for fractional melting models):

$$C_0^{H_2O} = C_{melt}^{H_2O} \cdot (D + f \cdot (1 - D)) \quad (5)$$

$$C_0^{H_2O} = C_{melt}^{H_2O} \cdot f / \left(1 - (1 - f)^{1/D}\right) \quad (6)$$

$C_0^{H_2O}$ represents the concentration of water in the mantle source, D is the partition coefficient between the basaltic melt and the peridotitic source, and f is the degree of partial melting.

The partition coefficient for water between the peridotitic source and basaltic melt, which were used (between 0.005 and 0.013), are those of Aubaud et al. (2004), Hirschmann et al. (2009), Tenner et al. (2009) and Hao et al. (2014). Unfortunately, there is no exact value in the literature regarding the degree of partial melting below the Gutâi Volcanic Zone. Therefore, data from Seghedi et al. (1995) was used as it presents the partial melting degree for the whole Eastern Carpathians. The data from Kushiro (2007) was employed as it was derived from geodynamic setting similar to that of the Eastern Carpathians. The degree of partial melting in the mantle used for the calculations was estimated to be between 10 and 15 % based on the aforementioned literature.

The water content of the mantle source was calculated using the calculated melt water contents with an error margin of 10 %. Furthermore, the partition coefficient of 0.005, 0.007, 0.009, 0.011, and 0.013, as well as the degree of partial melting of 10, 12.5, and 15 %, were considered. The source 'water' contents were calculated for all variations of the parameters for each selected sample, in order to present all possible results (for further details, please refer to Supplemet S9).

Discussion

Petrogenetic explanation

Clinopyroxenes are among the most suitable minerals for the documentation of complex magma evolutions in terms of their compositional and structural features. The calculated pressures and temperatures of the clinopyroxene pheno- and glomerocryst cores from the FBC reveal the crystallisation conditions and the nature of their parental melt.

The thermobarometric data of the studied clinopyroxenes indicate that they crystallised in a deep magma chamber (22–30 km depth), in agreement with the model presented by Kovacs et al. (2021) for the FBC magmatic plumbing system.

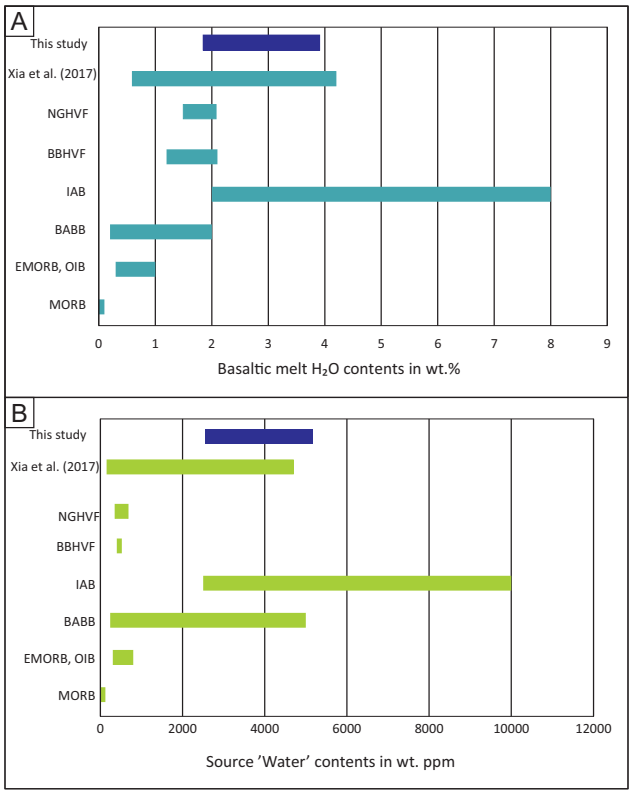

Fig. 8. The calculated equilibrium 'water' content of the FBC basalts (**A**) in wt.% compared to the literature values (Dixon et al. 2004; Xia et al. 2017; Kovács et al. 2020). For details of the calculations see 'Water' content of the basaltic melt in equilibrium with the clinopyroxenes and Supplement S9. The calculated source 'water' content for the FBC basalts (**B**) in wt. ppm compared to the other references (Dixon et al. 2004; Xia et al. 2017; Kovács et al. 2020). For details of the calculations see Supplement S9

The high Mg# (79–91) cores of the clinopyroxene phenocrysts and glomerocrysts were among the early phases to crystallise in the deepest magma reservoir at the bottom of the lower crust (MOHO in the GVZ is at 33–35 km depth, Săndulescu et al. 1993; Bielik et al. 2018; Kovacs et al. 2021). The presence of the similarly high Mg# (75–85) olivine phenocrysts in some clinopyroxene clusters (Fig. 2D; Supplement S2A,B) indicates that the two minerals crystallised as the initial phases from a primitive basaltic melt. The data presented here are in accordance with the experimental data of Ulmer et al. (2018), in which the first crystallised phase was olivine, followed by clinopyroxene, starting from a high-Mg basalt composition (at P=10 kbar). In this experiment, the temperature range for the crystallisation of the high Mg# clinopyroxenes was 1080–1170 °C, which is comparable to the temperatures calculated for the FBC clinopyroxenes (1100–1170 °C).

In a recent experiment, Marxer et al. (2022) utilised as a starting material some derivative liquids derived from the fractional crystallisation experimental study of Ulmer et al. (2018) conducted on a primitive high-Mg basalt at 10 kbar. The experiment demonstrated that olivine and clinopyroxene are the initial phases to crystallise within the pressure range of 10–6 kbar and temperature range of 1170–1080 °C, where plagioclase forms at a pressure of less than 6 kbar and a temperature of less than 1050 °C. The experimental clinopyroxenes exhibit a range of compositions, including diopside and augite. In the experimental run, the initial starting material was held at equilibrium with olivine and clinopyroxene at 1170 °C and 10 kbar (by decreasing the pressure and temperature by a step of 2 kbar and 60 °C respectively). The formation of clinopyroxene occurred at 8 kbar and 1110 °C, exhibiting a similar composition ($Wo_{45}En_{47}Fs_{8}$) to that observed in the investigated clinopyroxenes from Firiza basalts ($Wo_{41–51}En_{39–51}Fs_{4–14}$).

The chemical composition of the clinopyroxenes from the Firiza basalts indicates that the clinopyroxene cores of the phenocrysts and glomerocrysts are the most primitive, having crystallised from the most primitive basaltic melt of the FBC magmatic plumbing system. The overall normal zoning observed in the studied clinopyroxenes (with consistently highest MgO, CaO, and Cr_2O_3 and lowest FeO in the phenocryst and glomerocryst cores) indicates that fractional crystallisation was the primary magmatic process involved in their formation. The compositional recurrences observed in the transitional zones (Supplements S10, S11) indicate the potential involvement of crystal convection and magma recharge processes in deep magma reservoirs of the FBC plumbing system. The model of Kovacs et al. (2021) indicates that the principal magmatic processes occurred in the lower crustal magma reservoirs, which are exclusively composed of the volcanic plumbing system of the FBC. These magmas ascended relatively rapidly towards the surface, forming small intrusions.

The water content of the melts from which the clinopyroxenes were formed has been investigated in both thermobarometric and experimental studies. Ulmer et al. (2018) measured a higher H_2O content (4.3–5.2 wt.%) in their experimental melt, in which the clinopyroxenes formed at 10 kbar and 1140–1200 °C, using Raman spectrometry. The water content measured by Marxer et al. (2022) in the melt in which the clinopyroxenes formed at 8 kbar and 1110 °C (compositional similar with FBC clinopyroxenes) was 3.2 wt.% H_2O. In the most recent experimental study, Blatter et al. (2023) measured a content of 1.95–2.05 wt.% H_2O in the post-run samples (synthesised glasses from the melt with clinopyroxenes) analysed with FTIR spectroscopy at P=9 kbar, starting from a Cascade Range calc-alkaline basalt.

'Water' content in the Firiza basaltic melt and its source region

In the clinopyoxene pheno- and glomerocrysts from the Firiza basalts, the three most notable absorption bands on the FTIR spectra (Fig. 7) could be attributed to the following substitutions in their structure: the bands around 3630 cm^{-1} are connected to OH^- in T [Si] vacancy or coupled $Na^+ + H^+ \leftrightarrow M$ substitution (octahedral site, Bromiley et al. 2004; Stalder & Ludwig 2007). The bands around 3520 cm^{-1} are connected to the $Al^{3+} + H^+ \leftrightarrow Si^{4+}$ substitution (Koch-Müller et al. 2004),

whereas the bands around 3470 cm^{-1} are attributed to the OH^- in octahedral (M2) vacancy (Smyth et al. 1991).

In the studied samples, there are absorption bands observed at ~3640 cm^{-1}, ~3515 cm^{-1}, and 3465 cm^{-1} (Fig. 7). Comparing the spectra with those of Kovács et al. (2016, 2020) and Patkó et al. (2019) (Fig. 7B) the band around 3630 cm^{-1} is situated at a higher wavenumber (approximately +10 cm^{-1}) and has much higher intensity. With regard to the bands situated at approximately 3520 cm^{-1} in our samples, it can be observed that the absorption is more pronounced at lower wavenumbers, specifically around 3515 cm^{-1}. Furthermore, the bands situated at approximately 3465 cm^{-1} are also more pronounced.

The structural hydroxyl content of the studied FBC clinopyroxenes can be seen, in comparison to values from previous studies in Fig. 9, and detailed below. The structural hydroxyl content measured from the FBC clinopyroxenes can be considered higher than the values reported from alkali basalts and mantle xenoliths by Liu et al. (2015); Kovács et al. (2016); Patkó et al. (2019), those reported by Weis et al. (2015) before rehydration and a few from Wade et al. (2008), but after rehydration the data of (Weis et al. 2015),the rest from Wade et al. (2008) and from Patkó et al. (2025) is overlapping with the FBC values. The rest of the literature data (Nazzareni et al. 2008, 2011; Okumura 2011; Lloyd et al. 2016; Turner et al. 2017; Radu et al. 2023), are in the same range as the ones measured in the FBC.

The 'water' content of the Firiza basaltic melt in equilibrium with the clinopyroxene phenocrysts was calculated based on their structural hydroxyl content and chemical composition using the method of O'Leary et al. (2010), as outlined in Equation (2–4).

The fractionation-corrected 'water' content (1.85–3.91 wt.% H_2O) is in good agreement with global values for arc magmas (2–8 wt.% H_2O) and higher than the MORB, OIB and BABB values reported by Dixon et al. (2004) (Fig. 8A, Supplement S8). The 'water' content in the FBC (1.85–3.91 wt.% H_2O) is relatively close to the proposed 'water' content (~3.5 wt.% H_2O) for mantle melts from the mantle wedge conditions: 1250–1300 °C and 1.5 GPa (Plank et al. 2013). Collins et al. (2020) provide a model for the eruption of (~4 wt.% H_2O) mafic arc magmas to the surface, which may be the case for the FBC, and the stalling of more hydrous melts at the IAB. Grove et al. (2012) reported magma 'water' contents for arc melts ranging from 0 to 6–7 wt.% H_2O, where 6–7 wt.% H_2O corresponds to vapour saturation of basaltic magmas at shallow depths (6–8 km), which is not the case for the Firiza basalts as they did not stall at shallower depths. Comparing the data of this work with results obtained by similar methods, it is higher than the values reported by Kovács et al. (2016, 2020) from the BBHVF alkali basalts (1.2–2.1 wt.%) and Patkó et al. (2025) from the NGVF alkali basalts (1.5–2.08 wt.%) (Fig. 8A, Supplement S8) and higher than most of the data reported by Xia et al. (2017) from alkali basalts in eastern China (0.6–4.2 wt.%) Although other works from the CPR (Cserép et al. 2023; Seghedi et al. 2023) reported higher 'water' contents (8–10 %) it is based on the presence or absence of particular hydrous minerals and it is only an indirect way to obtain a semiquantitative 'water' content therefore in our opinion it not the most suitable dataset for a direct comparison with our results.

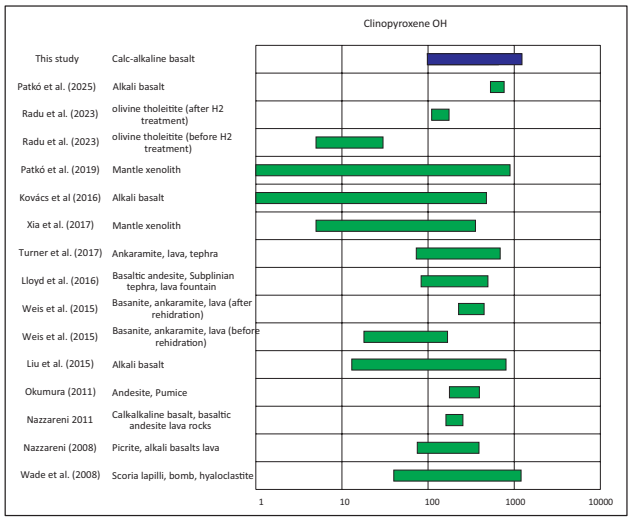

Fig. 9. The structural hydroxyl content of the measured clinopyroxenes in wt. ppm on logarithmic scale compared to the literature values (Nazzareni et al. 2008, 2011; Wade et al. 2008; Okumura 2011; Xia et al. 2013a; Liu et al. 2015; Weis et al. 2015; Kovács et al. 2016; Lloyd et al. 2016; Turner et al. 2017; Patkó et al. 2019; Radu et al. 2023)

In the source 'water' content calculations it can be observed that the variation of the partition coefficient has a significant effect on the modal batch melting model (Equation 5) compared to the modal fractional melting model (Equation 6), where it has an almost negligible effect, with a higher partition coefficient resulting in a higher source 'water' content. Changing the degree of partial melting has a similar effect on both models, as the higher degree of partial melting results in a higher source 'water' content. The modal batch model also gives higher source water contents than the modal fractional model for the same parameters. The largest effect can be attributed to the $C_{melt}^{H_2O}$ variations in the calculations, which are the result of previous experimental studies and also influenced by the fractionation and structural hydroxyl content determinations (for details see Supplement S9). The resulting 'water' contents are shown in Fig. 8B and Fig. 10.

The calculated source 'water' content of ~2200–5200 wt. ppm in light of literature data is in the range of the IAB source region of 2500–10,000 ppm (Dixon et al. 2004) and much higher than the 400–520 ppm reported by Kovács et al. (2020) from the BBHVF region and the 400–700 ppm reported by Patkó et al. (2025) (Fig. 8B).

Xia et al. (2017) investigated alkali basalts from eastern China for their melt 'water' content and the 'water' content of their source region. They reported 'water' contents from the source region of the eastern China area up to 6000 wt. ppm, most of them ~2000–2500 wt. ppm, while from the western area only up to 1500 wt. ppm (Fig. 8B). They explain this

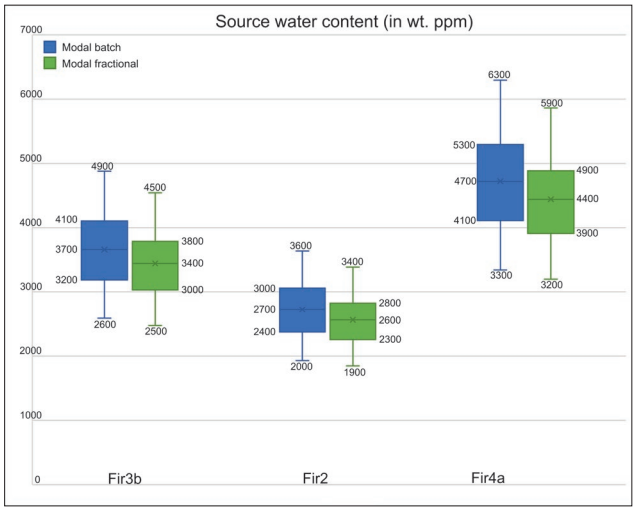

Fig. 10. The calculated source 'water' contents for the 3 selected samples. Both the modal batch and modal fractional model calculations are presented here. For these the melting degrees were changed between 10–15 %, the partition coefficient between 0.005–0.013, and the assumed fractionation was 20 %. The diagram displays the median and mean of the whole dataset, the medians of both the bottom and top half of the data set, and the minimum and maximum points with their values displayed beside them.

difference with the effect of Pacific plate subduction, which is responsible for the heterogeneities seen in the upper mantle and mantle transition zone beneath the region.

The high magmatic and source 'water' contents determined in this work for the FBC relative to the alkali basalts in the central part of the CPR are attributed to the geodynamic situation of the GVZ. The alkaline basalts in the CPR erupted to the surface from the late Miocene to the Pleistocene (Embey-Isztin et al. 1993; Downes et al. 1995; Seghedi et al. 2004; Harangi & Lenkey 2007; Ali & Ntaflos 2011; Ali et al. 2013; Harangi et al. 2015). In the CPR, these alkali basalts occur both in the central parts and at the boundary of the CPR. The localities on the western and eastern border of the region (SBVF and PMVF) are in the vicinity of former subduction zones (Tondi et al. 2009; Dando et al. 2011; Mitterbauer et al. 2011; Ismail-Zadeh et al. 2012; Qorbani et al. 2015), whereas the other localities (LHPVF, BBHVF, NGVF) may have only been slightly affected by such recent processes. Liptai et al. (2021) studied the structural hydroxyl content of NAM's of mantle xenoliths from SBVF, BBHVF, NGVF and PMVF and found that the localities in the centre of the basin (BBHVF, NGVF) have low 'water' contents compared to those from the peripheral areas. According to their findings, the inner parts were less affected by recent subduction, whereas the western and eastern peripheral parts were metasomatised by recent and almost contemporaneous subduction in their vicinity. However, the asthenosphere appears to be wet even beneath the central part of the basin, which may be related to the hydrous mantle transition zone beneath the CPR (Kovács et al. 2020).

In comparison, the volcanism in the GVZ, although partially overlapping in time with the alkaline basalts, is in a post-collisional tectonic setting closely related to the recent subduction that occurred along the Eastern Carpathians. The Eastern Carpathians and also the GVZ are considered to have a subduction-influenced mantle source (e.g., Szabó et al. 1992; Seghedi et al. 1995; Harangi & Lenkey 2007; Kovacs et al. 2017). This is also supported by the chemical composition of the studied FBC basaltic rocks, which show a subduction-related elemental distribution, as discussed in the whole-rock geochemistry chapter. Therefore, the source region of the FBC should be affected by the subducting slab, increasing its 'water' content. This supports our observations and agrees with literature values (Dixon et al. 2004; Xia et al. 2017) and previous studies from the CPR (Kovács et al. 2020; Liptai et al. 2021; Patkó et al. 2025).

Summary

The clinopyroxenes of the calc-alkaline basalts of the FBC have been studied to analyse the structural hydroxyl content and to infer the 'water' content of the parent melt and source region. The FBC basalts show typical arc/subduction zone-related volcanism features, as does the volcanism of the GVZ as a whole.

This study focused on the chemistry of the clinopyroxene phenocrysts and glomerocrysts and their crystallisation P–T parameters. The chemical composition showed that the core of the phenocrysts and glomerocrysts is the most primitive (Mg#: 79–91). Based on the calculated P–T data (~5.5–8.5 kbar and 1100–1170 °C, respectively), deep magma source (22–30 km depth) in the lower crust, near the MOHO (33–35 km depth in the GVZ), was assumed for the early clinopyroxene crystallisation. They were formed from primitive basaltic melts at lower crustal levels and later emplaced in small intrusions without stalling in the lithosphere.

The structural hydroxyl contents of the clinopyroxene cores are relatively high (105–515 wt. ppm). Rapid emplacement and cooling of the small intrusions preserved the structural hydroxyl content of the clinopyroxenes in 4 of the 5 intrusive bodies studied. Their calculated equilibrium 'water' contents (1.85–3.91 wt. %) and source 'water' contents (2200–5200 wt. ppm) are in the range reported for the Island Arc basalts and higher than the range reported for the alkali basalts of the Bakony–Balaton Highland Volcanic Field. These results are in good agreement with the geodynamic setting of the FBC, which is in a post-collisional tectonic setting closely related to the subduction of the Eastern Carpathians. The subducting slab increased the 'water' content in the source region of the FBC in the GVZ, in contrast to the low water activity in the source region of the BBHVF alkaline basalts from the inner part of the Pannonian Basin. This is the first study of magmatic water in calc-alkaline volcanism in the CPR using the structural hydroxyl content of nominally anhydrous minerals (NAMs). In conclusion, the FBC calc-alkaline basalts are ideal occurrences to study equilibrium melt and source 'water' contents and to outline the effect of regional geody-

namics on melting processes from the source region in an inverted extensional basin.

Acknowledgements: This study was financially supported by the MTA FI Lendület Pannon LitH_2Oscope Research Group, the NKFIH K141956 Topo-Transylvania grant. This is the 125. publication of the Lithosphere Fluid Research Lab (LRG).

References

Ali S. & Ntaflos T. 2011: Alkali basalts from Burgenland, Austria: Petrological constraints on the origin of the westernmost magmatism in the Carpathian-Pannonian Region. *Lithos* 121, 176–188. https://doi.org/10.1016/j.lithos.2010.11.001

Ali S., Ntaflos T. & Upton B.G.J. 2013: Petrogenesis and mantle source characteristics of Quaternary alkaline mafic lavas in the western Carpathian-Pannonian Region, Styria, Austria. *Chemical Geology* 337–338, 99–113. https://doi.org/10.1016/j.chemgeo.2012.12.001

Asimow P.D., Dixon J.E. & Langmuir C.H. 2004: A hydrous melting and fractionation model for mid-ocean ridge basalts: Application to the Mid-Atlantic Ridge near the Azores. Geochemistry, *Geophysics, Geosystems* 5. https://doi.org/10.1029/2003GC000568

Aubaud C., Hauri E.H. & Hirschmann M.M. 2004: Hydrogen partition coefficients between nominally anhydrous minerals and basaltic melts. *Geophysical Research Letters* 31. https://doi.org/10.1029/2004GL021341

Bell D.R., Ihinger P.D. & Rossman G.R. 1995: Quantitative analysis of trace OH in garnet and pyroxenes. *American Mineralogist* 80, 465–474. https://doi.org/10.2138/am-1995-5-607

Bielik M., Makarenko I., Csicsay K., Legostaeva O., Starostenko V., Savchenko A., Šimonová B., Dérerová J., Fojtíková L., Pašteka R. & Vozár J. 2018: The refined Moho depth map in the Carpathian–Pannonian region. *Contributions to Geophysics and Geodesy* 48, 179–190.

Biró T., Kovács I., Király E., Falus G., Karátson D., Bendő Z., Fancsik T. & Sándor-Kovács J. 2016: Concentration of hydroxyl defects in quartz from various rhyolitic ignimbrite horizons: Results from unpolarized micro-FTIR analyses on unoriented phenocryst fragments. *European Journal of Mineralogy* 28, 313–327. https://doi.org/https://doi.org/10.1127/ejm/2016/0028-2515

Blatter D.I., Sisson T.W. & Hankins W.B. 2023: Garnet stability in arc basalt, andesite, and dacite-an experimental study. *Contributions to Mineralogy and Petrology* 178, 33. https://doi.org/10.1007/s00410-023-02008-w

Bromiley G., Keppler H., Mccammon C., Bromiley F. & Jacobsen S. 2004: Hydrogen solubility and speciation in natural, gem-quality chromian diopside. *American Mineralogist* 89, 941–949. https://doi.org/10.2138/am-2004-0703

Collins W.J., Murphy J.B., Johnson T.E. & Huang H.Q. 2020: Critical role of water in the formation of continental crust. *Nature Geoscience* 13, 331–338. https://doi.org/10.1038/s41561-020-0573-6

Cserép B., Szemerédi M., Harangi S., Erdmann S., Bachmann O., Dunkl I., Seghedi I., Mészáros K., Kovács Z., Virág A., Ntaflos T., Schiller D., Molnár K. & Lukács R. 2023: Constraints on the pre-eruptive magma storage conditions and magma evolution of the 56–30 ka explosive volcanism of Ciomadul (East Carpathians, Romania). *Contributions to Mineralogy and Petrology* 178, 96. https://doi.org/10.1007/s00410-023-02075-z

Csontos L. & Nagymarosy A. 1998: The mid-Hungarian line: a zone of repeated tectonic inversion. *Tectonophysics* 297, 51–71. https://doi.org/10.1016/S0040-1951(98)00163-2

Csontos L., Nagymarosy A., Horváth F. & Kovác M. 1992: Tertiary evolution of the Intra-Carpathian area: A model. *Tectonophysics* 208, 221–241. https://doi.org/10.1016/0040-1951(92)90346-8

Dando B.D.E., Stuart G.W., Houseman G.A., Hegedüs E., Brückl E. & Radovanović S. 2011: Teleseismic tomography of the mantle in the Carpathian–Pannonian region of central Europe. *Geophysical Journal International* 186, 11–31. https://doi.org/10.1111/J.1365-246X.2011.04998.X/3/186-1-11-FIG015.JPEG

Dixon J.E., Dixon T.H., Bell D.R. & Malservisi R. 2004: Lateral variation in upper mantle viscosity: Role of water. *Earth and Planetary Science Letters* 222, 451–467. https://doi.org/10.1016/j.epsl.2004.03.022

Dobosi G. & Jenner G.A. 1999: Petrologic implications of trace element variation in clinopyroxene megacrysts from the Nograd volcanic province, north Hungary: a study by laser ablation microprobe-inductively coupled plasma-mass spectrometry. *Lithos* 46, 731–749. https://doi.org/10.1016/S0024-4937(98)00093-0

Downes H., Seghedi I., Szakacs A., Dobosi G., James D.E., Vaselli O., Rigby I.J., Ingram G.A., Rex D. & Pécskay Z. 1995: Petrology and geochemistry of late Tertiary/Quaternary mafic alkaline volcanism in Romania. *Lithos* 35, 65–81.

Edelstein O., Pécskay Z., Kovacs M., Bernad A., Crihan M. & Micle R. 1993: The age of the basalts of the Firiza zone, Ignis Mts., East Carpathians, Romania. *Revue Roumaine de Geologie* 37, 45–60.

Embey-Isztin A., Downes H., James D.E., Upton B.G.J., Dobosi G., Ingram G.A., Harmon R.S. & Scharbert H.G. 1993: The petrogenesis of Pliocene alkaline volcanic rocks from the Pannonian Basin, Eastern Central Europe. *Journal of Petrology* 34, 317–343. https://doi.org/10.1093/petrology/34.2.317

Fülöp A. 2002: Facies analysis of the volcaniclastic sequence built up above the 15.4 Ma rhyolitic ignimbrites from Gutâi Mts., Eastern Carpathians. *Studia Universitatis Babeş-Bolyai Geologia Special issue* 1, 199–206.

Fülöp A. 2003: The begining of volcanism in the Gutâi Mts.: Paleovolcanic and paleosedimentological reconstruction. *Editura Dacia Cluj-Napoca*, 1–134 (in Romanian).

Gröger H.R., Fügenschuch B., Tischler M., Schmid S.M. & Foeken P.T. 2008: Tertiary cooling and exhumation history in the Maramures area (internal eastern Carpathians, northern Romania): thermochronology and structural data. In: Siegesmund S., Fügenschuch B. & Froitzheim N. (eds.): Tectonic Aspects of the Alpine–Dinaride–Carpathian System. *Geological Society of London Special Publications* 298, 169–195. https://doi.org/10.1144/SP298.9

Grove T.L., Till C.B. & Krawczynski M.J. 2012: The role of H_2O in subduction zone magmatism. *Annual Review of Earth and Planetary Sciences* 40, 413–439. https://doi.org/10.1146/annurev-earth-042711-105310

Hao Y., Xia Q., Li Q., Chen H. & Feng M. 2014: Partial melting control of water contents in the Cenozoic lithospheric mantle of the Cathaysia block of South China. *Chemical Geology* 380, 7–19. https://doi.org/10.1016/J.CHEMGEO.2014.04.017

Harangi S. & Lenkey L. 2007: Genesis of the neogene to quaternary volcanism in the Carpathian–Pannonian region: Role of subduction, extension, and mantle plume. *Special Paper of the Geological Society of America* 418, 67–92. https://doi.org/10.1130/2007.2418(04)

Harangi S., Jankovics M.É., Sági T., Kiss B., Lukács R. & Soós I. 2015: Origin and geodynamic relationships of the Late Miocene to Quaternary alkaline basalt volcanism in the Pannonian basin, eastern–central Europe. *International Journal of Earth Sciences* 104, 2007–2032. https://doi.org/10.1007/s00531-014-1105-7

Harangi S., Seghedi I. & Lukács R. 2024: The Neogene–Quaternary volcanism of the Carpathian–Pannonian region: from initial plate tectonic models to quantitative petrogenetic explanations. *Geological Society London, Special Publications* 554, SP554-2024.

Hirschmann M.M., Tenner T., Aubaud C. & Withers A.C. 2009: Dehydration melting of nominally anhydrous mantle: The primacy of partitioning. *Physics of the Earth and Planetary Interiors* 176, 54–68. https://doi.org/10.1016/J.PEPI.2009.04.001

Ismail-Zadeh A., Matenco L., Radulian M., Cloetingh S. & Panza G. 2012: Geodynamics and intermediate-depth seismicity in Vrancea (the south-eastern Carpathians): Current state-of-the art. *Tectonophysics* 530–531, 50–79. https://doi.org/10.1016/J.TECTO.2012.01.016

Irvine T.N. & Baragar W.R.A. 1971: A Guide to the Chemical Classification of the Common Volcanic Rocks. *Canadian Journal of Earth Sciences* 8, 523–548. https://doi.org/10.1139/e71-055

Koch-Müller M., Matsyuk S.S. & Wirth R. 2004: Hydroxyl in omphacites and omphacitic clinopyroxenes of upper mantle to lower crustal origin beneath the Siberian platform. *American Mineralogist* 89, 921–931. https://doi.org/10.2138/am-2004-0701

Kovács I., Hermann J., O'Neill H.S.C., Gerald J.F., Sambridge M. & Horváth G. 2008: Quantitative absorbance spectroscopy with unpolarized light, Part II: Experimental evaluation and development of a protocol for quantitative analysis of mineral IR spectra. *American Mineralogist* 93, 765–778. https://doi.org/10.2138/am.2008.2656

Kovács I., Demény A., Czuppon G., Lécuyer C., Fourel F., Xia Q.K., Liu J., Pintér Z., Király E., Török K., Szabó Á., Deloule E., Falus G., Fancsik T., Zajacz Z., Sándorné Kovács J. & Udvardi B. 2016: Water concentrations and hydrogen isotope compositions of alkaline basalt-hosted clinopyroxene megacrysts and amphibole clinopyroxenites: the role of structural hydroxyl groups and molecular water. *Contributions to Mineralogy and Petrology* 171, 38. https://doi.org/10.1007/s00410-016-1241-0

Kovács I., Patkó L., Liptai N., Lange T.P., Taracsák Z., Cloetingh S.A.P.L., Török K., Király E., Karátson D., Biró T., Kiss J., Pálos Z., Aradi L.E., Falus G., Hidas K., Berkesi M., Koptev A., Novák A., Wesztergom V., Fancsik T. & Szabó C. 2020: The role of water and compression in the genesis of alkaline basalts: Inferences from the Carpathian-Pannonian region. *Lithos* 354–355, 105323. https://doi.org/10.1016/j.lithos.2019.105323

Kovacs M. 2002: Petrogenesis of subduction-related igneous rocks from the central-southeastern area of the Gutâi Mts. *Editura Dacia Cluj-Napoca*, 1–201 (in Romanian).

Kovacs M. & Fülöp A. 2003: Neogene volcanism in the Gutâi Mts. (Eastern Carpathians): a review. *Studia Universitatis Babeş-Bolyai, Geologia* 48, 3–16.

Kovacs M., Pécskay Z., Fülöp A., Jurje M. & Edelstein O. 2013a: Geochronology of the Neogene intrusive magmatism of the Oas-Gutâi Mountains, Eastern Carpathians (NW Romania). *Geologica Carpathica* 64, 483–496. https://doi.org/10.2478/geoca-2013-0033

Kovacs M., Pécskay Z., Fülöp A., Jurje M. & Edelstein O. 2013b: Firiza basalts – the final stage of the Neogene calc-alkaline volcanic activity from Gutâi Volcanic Zone, Eastern Carpathians, Romania. In: Büchner J., Rapprich V. & Tietz O. (eds.): Basalt 2013, *Cenozoic Magmatism in Central Europe, Abstracts & Excursion Guides*, 88–89.

Kovacs M., Seghedi I., Yamamoto M., Fülöp A., Pécskay Z. & Jurje M. 2017: Miocene volcanism in the Oaş-Gutâi Volcanic Zone, Eastern Carpathians, Romania: Relationship to geodynamic processes in the Transcarpathian Basin. *Lithos* 294, 304–318. https://doi.org/10.1016/j.lithos.2017.09.027

Kovacs M., Fülöp A., Seghedi I. & Pécskay Z. 2021: Architecture of volcanic plumbing systems inferred from thermobarometry: A case study from the Miocene Gutâi Volcanic Zone in the Eastern Carpathians, Romania. *Lithos* 396–397, 106191. https://doi.org/10.1016/j.lithos.2021.106191

Kuno H. 1960: High-alumina basalt. *Journal of Petrology* 1, 121–145.

Kushiro I. 2007: Origin of magmas in subduction zones: a review of experimental studies. *Proceedings of the Japan Academy, Series B* 83, 1–15 https://doi.org/10.2183/pjab.83.1

Le Bas M.J., Le Maitre R.W., Streckeisen A. & Zanettin B. 1986: A chemical classification of volcanic rocks based on the total alkali-silica diagram. *Journal of Petrology* 27, 745–750. https://doi.org/https://doi.org/10.1093/petrology/27.3.745

Liptai N., Lange T.P., Patkó L., Pintér Z., Berkesi M., Aradi L.E., Szabó C. & Kovács I.J. 2021: Effect of water on the rheology of the lithospheric mantle in young extensional basin systems as shown by xenoliths from the Carpathian-Pannonian region. *Global and Planetary Change* 196, 103364. https://doi.org/10.1016/j.gloplacha.2020.103364

Liu J., Xia Q., Deloule E., Chen H. & Feng M. 2015: Recycled oceanic crust and marine sediment in the source of alkali basalts in Shandong, Eastern China: Evidence from magma water content and oxygen isotopes. *Journal of Geophysical Research: Solid Earth* 120, 8281–8303. https://doi.org/10.1002/2015JB012476

Liu S.C., Xia Q.K., Choi S.H., Deloule E., Li P. & Liu J. 2016: Continuous supply of recycled Pacific oceanic materials in the source of Cenozoic basalts in SE China: the Zhejiang case. *Contributions to Mineralogy and Petrology* 171, 1–31. https://doi.org/10.1007/s00410-016-1310-4

Lloyd A.S., Ferriss E., Ruprecht P., Hauri E.H., Jicha B.R. & Plank T. 2016: An assessment of clinopyroxene as a recorder of magmatic water and magma ascent rate. *Journal of Petrology* 57, 1865–1886. https://doi.org/https://doi.org/10.1093/petrology/egw058

Marxer F., Ulmer P. & Müntener O. 2022: Polybaric fractional crystallisation of arc magmas: an experimental study simulating trans-crustal magmatic systems. *Contributions to Mineralogy and Petrology* 177, 3. https://doi.org/10.1007/s00410-021-01856-8

Mollo S., Putirka K., Misiti K., Soligo M. & Scarlato P. 2013: A new test for equilibrium based on clinopyroxene-melt pairs: Clues on the solidification temperatures of Etnean alkaline melts at post-eruptive conditions. *Chemical Geology* 352, 92–100. https://doi.org/10.1016/j.chemgeo.2013.05.026

Morimoto N., Fabries J., Ferguson A.K., Ginzburg I.V., Ross M., Seifert F.A., Zussman J., Aoki K. & Gottardi G. 1988: Nomenclature of pyroxenes. *American Mineralogist* 73, 1123–1133.

Mitterbauer U., Behm M., Brückl E., Lippitsch R., Guterch A., Keller G.R., Koslovskaya E., Rumpfhuber E.M. & Sumanovac F. 2011: Shape and origin of the East-Alpine slab constrained by the ALPASS teleseismic model. *Tectonophysics* 510, 195–206. https://doi.org/10.1016/J.TECTO.2011.07.001

Nazzareni S., Pompilio M., Skogby H. & Zanazzi P.F. 2008: Water contents of pyroxenes from Etna recent eruptions. In: *AGU Fall Meeting Abstracts*, V21B-2109.

Nazzareni S., Skogby H. & Zanazzi P.F. 2011: Hydrogen content in clinopyroxene phenocrysts from Salina mafic lavas (Aeolian Arc, Italy). *Contributions to Mineralogy and Petrology* 162, 275–288. https://doi.org/https://doi.org/10.1007/s00410-010-0594-z

Neave D.A. & Putirka K.D. 2017: A new clinopyroxene-liquid barometer, and implications for magma storage pressures under Icelandic rift zones. *American Mineralogist* 102, 777–794. https://doi.org/10.2138/am-2017-5968

O'Leary J.A., Gaetani G.A. & Hauri E.H. 2010: The effect of tetrahedral Al^{3+} on the partitioning of water between clinopyroxene and silicate melt. *Earth and Planetary Science Letters* 297, 111–120. https://doi.org/10.1016/j.epsl.2010.06.011

Okumura S. 2011: The H_2O content of andesitic magmas from three volcanoes in Japan, inferred from the infrared analysis of clinopyroxene. *European Journal of Mineralogy* 23, 771–778. https://doi.org/https://doi.org/10.1127/0935-1221/2011/0023-2141

Patkó L., Liptai N., Kovács I.J., Aradi L.E., Xia Q.K., Ingrin J., Mihály J., O'Reilly S.Y., Griffin W.L., Wesztergom V. & Szabó C. 2019: Extremely low structural hydroxyl contents in upper mantle xenoliths from the Nógrád-Gömör Volcanic Field (northern Pannonian Basin): Geodynamic implications and the role of post-eruptive re-equilibration. *Chemical Geology* 507, 23–41. https://doi.org/10.1016/j.chemgeo.2018.12.017

Patkó L., Kővágó Á., Huraiová M., Kövér S., Gergely S., Konečný P. & Hurai V. 2025: Hydrous Asthenosphere Underneath the Northern Pannonian Basin. *Terra Nova*. https://doi.org/10.1111/ter.12763

Peccerillo A. & Taylor S.R. 1976: Geochemistry of eocene calc-alkaline volcanic rocks from the Kastamonu area, Northern Turkey. *Contributions to Mineralogy and Petrology* 58, 63–81. https://doi.org/10.1007/BF00384745

Pécskay Z., Lexa J., Szakács A., Seghedi I., Balogh K., Konečný V., Zelenka T., Kovács M., Póka T., Fülöp A., Márton E., Panaiotu C. & Cvetkovic V. 2006: Geochronology of Neogene magmatism in the Carpathian arc and intra-Carpathian area. *Geologica Carpathica* 57, 511–530.

Plank T., Kelley K.A., Zimmer M.M., Hauri E.H. & Wallace P.J. 2013: Why do mafic arc magmas contain ~4wt.% water on average? *Earth and Planetary Science Letters* 364, 168–179. https://doi.org/10.1016/j.epsl.2012.11.044

Putirka K. 2008: Thermometers and Barometers for Volcanic Systems. *Reviews in Mineralogy and Geochemistry* 69, 61–120. https://doi.org/10.2138/rmg.2008.69.3

Qorbani E., Bianchi I. & Bokelmann G. 2015: Slab detachment under the Eastern Alps seen by seismic anisotropy. *Earth and Planetary Science Letters* 409, 96–108. https://doi.org/10.1016/J.EPSL.2014.10.049

Radu I.B., Skogby H., Troll V.R., Deegan F.M., Geiger H., Müller D. & Thordarson T. 2023: Water in clinopyroxene from the 2021 Geldingadalir eruption of the Fagradalsfjall Fires, SW-Iceland. *Bulletin of Volcanology* 85, 31. https://doi.org/10.1007/s00445-023-01641-4

Saal A.E., Hauri E.H., Langmuir C.H. & Perfit M.R. 2002: Vapour undersaturation in primitive mid-ocean-ridge basalt and the volatile content of Earth's upper mantle. *Nature* 419, 451–455. https://doi.org/10.1038/nature01073

Sambridge M., Gerald J.F., Kovács I., O'Neill H.S.C. & Hermann J. 2008: Quantitative absorbance spectroscopy with unpolarized light: Part I. Physical and mathematical development. *American Mineralogist* 93, 751–764. https://doi.org/10.2138/am.2008.2657

Săndulescu M., Visarion M., Stănică D., Stănică M. & Atanasiu L. 1993: Deep structure of the Inner Carpathians in the Maramureş-Tisa zone (East Carpathians). *Romanian Journal of Geophysics* 16, 67–76 (in Romanian).

Seghedi I. & Downes H. 2011: Geochemistry and tectonic development of Cenozoic magmatism in the Carpathian–Pannonian region. *Gondwana Research* 20, 655–672. https://doi.org/10.1016/j.gr.2011.06.009

Seghedi I., Szakács A. & Mason P.R.D. 1995: Petrogenesis and magmatic evolution in the East Carpathian Neogene volcanic arc (Romania). *Acta Vulcanologica* 7, 135–143. https://www.researchgate.net/publication/312469544

Seghedi I., Downes H., Vaselli O., Szakács A., Balogh K. & Pécskay Z. 2004: Post-collisional Tertiary-Quaternary mafic alkalic magmatism in the Carpathian-Pannonian region: A review. *Tectonophysics* 393, 43–62. https://doi.org/10.1016/j.tecto.2004.07.051

Seghedi I., Lukács R., Soós I., Guillong M., Bachmann O., Cserép B. & Harangi S. 2023: Magma evolution in a complex geodynamic setting, South Harghita volcanic area, East-Central Europe: constraints from magma compositions and zircon petrochronology. *Lithos* 442, 107059. https://doi.org/10.1016/j.lithos.2023.107059

Smyth J., Bell D. & Rossman G. 1991: Incorporation of hydroxyl in upper-mantle clinopyroxenes. *Nature* 351, 732–735. https://doi.org/10.1038/351732a0

Stalder R. & Ludwig T. 2007: OH incorporation in synthetic diopside. *European Journal of Mineralogy* 19, 373–380. https://doi.org/10.1127/0935-1221/2007/0019-1721

Szabó C., Harangi S. & Csontos L. 1992: Review of Neogene and Quaternary volcanism of the Carpathian-Pannonian region. *Tectonophysics* 208, 243–256.

Tenner T.J., Hirschmann M.M., Withers A.C. & Hervig R.L. 2009: Hydrogen partitioning between nominally anhydrous upper mantle minerals and melt between 3 and 5 GPa and applications to hydrous peridotite partial melting. *Chemical Geology* 262, 42–56.

Tischler M., Gröger H.R., Fügenschuh B. & Schmid S.M. 2007: Miocene tectonics of the Maramures area (northern Romania): implications for the mid-Hungarian fault zone. *International Journal of Earth Sciences* 96, 473–496. https://doi.org/10.1007/s00531-006-0110-x

Tischler M., Mațenco L., Filipescu S., Gröger H.R., Wetzel A. & Fügenschuh B. 2008: Tectonics and sedimentation during convergence of the ALCAPA and Tisza-Dacia continental blocks: the Pienide nappe emplacement and its foredeep (N. Romania). In: Siegesmund S., Fügenschuch B. & Froitzheim N. (eds.): Tectonic Aspects of the Alpine-Dinaride-Carpathian System. *Geological Society of London Special Publications* 298, 317–334. https://doi.org/10.1144/SP298.15

Tondi R., Achauer U., Landes M., Daví R. & Besutiu L. 2009: Unveiling seismic and density structure beneath the Vrancea seismogenic zone, Romania. *Journal of Geophysical Research: Solid Earth* 114, B11. https://doi.org/10.1029/2008JB005992

Turner M., Turner S., Mironov N., Portnyagin M. & Hoernle K. 2017: Can magmatic water contents be estimated from clinopyroxene phenocrysts in some lavas? A case study with implications for the origin of the Azores Islands. *Chemical Geology* 466, 436–445. https://doi.org/10.1016/j.chemgeo.2017.06.032

Ubide T. & Kamber B.S. 2018: Volcanic crystals as time capsules of eruption history. *Nature Communications* 9, 326. https://doi.org/10.1038/s41467-017-02274-w

Ubide T., Mollo S., Zhao J., Nazzari M. & Scarlato P. 2019: Sector-zoned clinopyroxene as a recorder of magma history, eruption triggers, and ascent rates. *Geochimica et Cosmochimica Acta* 251, 265–283. https://doi.org/10.1016/j.gca.2019.02.021

Ulmer P., Kaegi R. & Müntener O. 2018: Experimentally Derived Intermediate to Silica-rich Arc Magmas by Fractional and Equilibrium Crystallization at 1·0 GPa: an Evaluation of Phase Relationships, Compositions, Liquid Lines of Descent and Oxygen Fugacity. *Journal of Petrology* 59, 11–58. https://doi.org/10.1093/petrology/egy017

Wade J.A., Plank T., Hauri E.H., Kelley K.A., Roggensack K. & Zimmer M. 2008: Prediction of magmatic water contents via measurement of H_2O in clinopyroxene phenocrysts. *Geology* 36, 799–802. https://doi.org/https://doi.org/10.1130/G24964A.1

Weis F.A., Skogby H., Troll V.R., Deegan F.M. & Dahren B. 2015: Magmatic water contents determined through clinopyroxene: Examples from the Western Canary Islands, Spain. *Geochemistry Geophysics Geosystems* 16, 2127–2146. https://doi.org/10.1002/2015GC005800

Wood D., Tarney J. & Weaver B. 1981: Trace element variations in Atlantic Ocean basalts and Proterozoic dykes from northwest Scotland: Their bearing upon the nature and geochemical evolution of the upper mantle. *Tectonophysics* 75, 91–112. https://doi.org/10.1016/0040-1951(81)90211-0

Xia Q.K., Hao Y.T., Liu S.C., Gu X.Y. & Feng M. 2013a: Water contents of the Cenozoic lithospheric mantle beneath the western part of the North China Craton: Peridotite xenolith constraints. *Gondwana Research* 23, 108–118. https://doi.org/10.1016/j.gr.2012.01.010

Xia Q.K., Liu J., Liu S.-C., Kovács I., Feng M. & Dang L. 2013b: High water content in Mesozoic primitive basalts of the North China Craton and implications on the destruction of cratonic mantle lithosphere. *Earth and Planetary Science Letters* 361, 85–97. https://doi.org/10.1016/j.epsl.2012.11.024

Xia Q.K., Liu J., Kovács I., Hao Y.T., Li P., Yang X.Z., Chen H. & Sheng Y.M. 2017: Water in the upper mantle and deep crust of eastern China: Concentration, distribution and implications. *National Science Review* 6, 125–144. https://doi.org/10.1093/nsr/nwx016

Electronic supplementary material is available online:
Supplements S1–S12 at https://geologicacarpathica.com/data/files/supplements/GC-76-1-Kovago_Supplements.zip